

# Causes of high O<sub>3</sub> in the lower free troposphere over the Pacific Northwest as observed at the Mt. Bachelor Observatory

J.L. Ambrose <sup>a,\*</sup>, D.R. Reidmiller <sup>b,1</sup>, D.A. Jaffe <sup>a,b</sup>

<sup>a</sup> Science and Technology Program, University of Washington-Bothell, Box 358581, 18115 Campus Way Northeast, Bothell, WA 98011, USA

<sup>b</sup> Department of Atmospheric Sciences, University of Washington, 408 Atmospheric Sciences-Geophysics (ATG) Building, Box 351640, Seattle, WA 98195, USA

## ARTICLE INFO

### Article history:

Received 31 March 2011

Received in revised form

18 June 2011

Accepted 18 June 2011

### Keywords:

Ozone

Pacific Northwest

Upper troposphere

Lower stratosphere

Asian long-range transport

Total atmospheric mercury

## ABSTRACT

We measured O<sub>3</sub>, CO, Hg, sub-micron particle scattering of mid-visible light ( $\sigma_{sp}$ ), and water vapor (WV) at the Mt. Bachelor Observatory (MBO) in central Oregon, USA since 2004. The data were used to identify sources of large ozone enhancements in the lower free troposphere (FT). A total of 25 high-ozone events, defined as time periods when the 8-h averaged O<sub>3</sub> mixing ratio was >70.0 ppbv, were recorded. The events occurred between early March and late September. For 18 of the 25 event days we were able to identify sources based on (1) relative enhancements of O<sub>3</sub>, CO, Hg and WV compared with the corresponding monthly distributions and (2) supporting data from the Hybrid Single-Particle Lagrangian Integrated Trajectory (HYSPPLIT) model, the Navy Aerosol Analysis and Prediction System (NAAPS) global aerosol model, and Moderate Resolution Imaging Spectroradiometer (MODIS) satellite-derived active fire counts from the Fire Information for Resource Management System (FIRMS). Our analysis suggests that enhanced O<sub>3</sub> levels during all the identified events were transported to MBO in the FT and were driven mostly by subsidence of O<sub>3</sub>-rich air masses from the upper troposphere/lower stratosphere (UT/LS), Asian long range transport (ALRT) and mixed ALRT + UT/LS influences. The UT/LS events were depleted in CO and total atmospheric mercury (TAM) compared to monthly median values. Levels of O<sub>3</sub> and CO tended to be anti-correlated during UT/LS events, consistent with transport from clean regions in the UT. Conversely, the ALRT events were characterized by concomitant enhancements in CO and TAM with mean values during each event that were >70th percentile values for the months during which the events occurred. Unlike for UT/LS events, levels of O<sub>3</sub> and CO during ALRT events tended to be correlated, consistent with photochemical O<sub>3</sub> production in polluted air masses transported across the Pacific. The mixed ALRT + UT/LS events exhibited characteristics that were intermediate between those of the ALRT and UT/LS events. For the classifiable cases the fractional distribution of each event type was: UT/LS, ~44% ( $n=8$ ); ALRT + UT/LS, ~33% ( $n=6$ ); ALRT, ~22% ( $n=4$ ). In terms of the total number of classifiable high-ozone event hours UT/LS, ALRT + UT/LS and ALRT events accounted for ~52% ( $t=85$ ), ~36% ( $t=59$ ) and ~13% ( $t=21$ ), respectively. The results indicate that downward mixing of O<sub>3</sub>-rich air masses from the UT/LS together with trans-Pacific transport of urban/industrial and biomass burning emissions from the Asian continent are the most important mechanisms for delivering high O<sub>3</sub> levels (i.e., 8-h averages >70.0 ppbv) to the lower FT in the Pacific Northwest.

© 2011 Elsevier Ltd. All rights reserved.

**Abbreviations:** ALRT, Asian long range transport; BB, biomass burning; BL, boundary layer; ER, enhancement ratio; FT, free troposphere; GEM, gaseous elemental mercury; LS, lower stratosphere; MBO, Mt. Bachelor Observatory; MFR, Medford, Oregon; NABB, North American biomass burning; NAI, North American industry; PHg, particulate mercury; PNW, Pacific Northwest; RGM, reactive gaseous mercury; SLE, Salem, Oregon; STE, stratosphere–troposphere exchange; TAM, total atmospheric mercury; TF, tropopause folding; TPP, tropopause pressure; UT, upper troposphere; WV, water vapor.

\* Corresponding author. Tel.: +1 425 352 3533; fax: +1 425 352 3775.

E-mail address: [jlambros@u.washington.edu](mailto:jlambros@u.washington.edu) (J.L. Ambrose).

<sup>1</sup> Currently in Washington, D.C. serving as a Congressional Science Fellow sponsored by the American Meteorological Society (AMS) and the University Corporation for Atmospheric Research (UCAR).

## 1. Introduction

A positive trend in tropospheric O<sub>3</sub> mixing ratios was recently reported both in the western Pacific region and over the western U.S. based on measurements from (1) several surface air monitoring stations in the western U.S. during 1987–2004 (Jaffe and Ray, 2007); (2) Mt. Happon, Japan during 1998–2007 (Tanimoto, 2009; Tanimoto et al., 2009); and (3) multiple atmospheric monitoring platforms over the U.S. west coast during 1984–2009 (Cooper et al., 2010). Concurrently, continued study of the impacts of O<sub>3</sub> exposure on human health have identified deleterious effects at progressively

lower exposure levels, leading regulatory agencies to consider the implementation of tighter standards for ground-level O<sub>3</sub> (EPA, 2010; Kim et al., 2011). For instance, the U.S. Environmental Protection Agency (EPA) is expected to lower the national ambient air quality standard (NAAQS) for O<sub>3</sub> from the current value of 75 ppbv to a value within the range of 60–70 ppbv (EPA, 2010). The combination of increasing baseline O<sub>3</sub> (i.e., the O<sub>3</sub> levels measured in air masses minimally influenced by recent anthropogenic emissions of O<sub>3</sub> precursors from North America (McDonald-Buller et al., submitted for publication; NRC, 2010)), together with tightening regulatory standards could complicate attainment of the standards in some parts of the country. This situation reinforces the importance, from scientific, environmental health and regulatory perspectives, of determining the factors which lead to elevated O<sub>3</sub> levels, both in the free troposphere (FT) and at the surface. While model analyses have identified the intensification of Asian anthropogenic emissions during the past two decades as a primary cause of (1) rising springtime O<sub>3</sub> levels in the western Pacific lower FT (Tanimoto et al., 2009) and (2) increasing summertime baseline O<sub>3</sub> levels over the continental U.S. (Fiore et al., 2002), it appears that the magnitudes of the Asian emissions increase and export to the western Pacific are not fully captured in the models (Tanimoto et al., 2009).

The Mt. Bachelor Observatory (MBO) in central Oregon, USA is uniquely positioned for characterizing the composition of the baseline FT near the U.S. west coast as well as perturbations from regional and distant sources. Previous studies at MBO have identified three distinct pollution influences: Asian long range transport (ALRT), North American biomass burning (NABB), and (more rarely) North American industry (NAI) (Jaffe et al., 2005; Weiss-Penzias et al., 2007; Reidmiller et al., 2010). Jaffe et al. (2005) determined that the total atmospheric mercury (TAM)/CO enhancement ratio (ER) can be used as a chemical signature for ALRT pollution plumes. Weiss-Penzias et al. (2006, 2007) extended this analysis to quantify the influence of Asian and biomass burning (BB) emissions on Hg and other pollutants at MBO. Swartzendruber et al. (2006) revealed that, at MBO, FT air masses tend to have large amounts of reactive gaseous mercury (RGM, thought to be composed primarily of Hg(II) species) whereas, boundary layer (BL)-influenced air masses tend to have far less of this form of Hg. Wolfe et al. (2007) measured acyl peroxy nitrates to detect ALRT plumes during the NASA INTEX-B mission (April–May 2006). Reidmiller et al. (2009) compared the interannual variability of ALRT events at MBO from spring 2005 to spring 2006 and determined that it was primarily controlled by Asian BB and Pacific transport patterns. Finley et al. (2009) quantified the amount of particulate mercury (PHg) emitted from regional (Pacific Northwest, PNW) wildfires and found that it was ~15% of the total Hg emitted from these fires. Fischer et al. (2010a) measured peroxyacetyl nitrate (PAN) at MBO during spring 2008 and characterized the synoptic conditions and O<sub>3</sub> production in several ALRT plumes. Reidmiller et al. (2010) analyzed the contributions of ALRT, NABB and NAI sources to high NO<sub>x</sub> (≡NO + NO<sub>2</sub>) levels at MBO.

There is considerable evidence that O<sub>3</sub> transport from the upper troposphere/lower stratosphere (UT/LS), as well as trans-Pacific transport of O<sub>3</sub> and its precursors from the Asian continent can significantly impact O<sub>3</sub> along the U.S. west coast (Jacob et al., 1999; Jaffe et al., 2004; Yienger et al., 2000; Cooper et al., 2010; Langford et al., 2010). Stratospheric influence on middle and upper tropospheric O<sub>3</sub> levels may be significant over the western U.S. during spring and early summer. For instance, an average 5 ppbv negative bias (model – observations) in GEOS-Chem modeled O<sub>3</sub> levels as compared with measurements made by the NCAR C-130 over the North American west coast during INTEX-B was attributed to an incomplete resolution of stratospheric influence in the model (Zhang et al., 2008). An analysis of ozonesonde profiles recorded at

Trinidad Head, California (THD) during 1997–2002 provided evidence that FT O<sub>3</sub> enhancements from winter to early summer are strongly influenced by stratosphere–troposphere exchange (STE) (referred to also as stratosphere to troposphere transport (STT) in the literature) (Newchurch et al., 2003). Stratospheric intrusions were found to contribute to several mid-tropospheric O<sub>3</sub> enhancements observed in ozonesonde profiles at THD and via airborne lidar over southern California during the CalNex mission (May–July 2010) (Langford et al., 2010). A recent study illustrating the influence of STE on global tropospheric ozone during 2005 indicated that fluxes of stratospheric O<sub>3</sub> into the troposphere were greatest during June, with maxima over North America and northeast Asia. Tropopause folding (TF), which is a primary mechanism of STE was greatest in June along the northern hemisphere (NH) subtropical jet (~30 °N), particularly over the eastern Pacific Ocean (Tang and Prather, 2010). Similarly, earlier studies determined that STE in the NH is greatest from late winter to early summer, and exhibits a maximum over the U.S. west coast (Kentarchos and Roelofs, 2003; Sprenger and Wernli, 2003).

It is well known that levels of trace gas and particulate pollutants throughout the tropospheric column over the U.S. west coast are enhanced by trans-Pacific transport of urban/industrial and BB emissions from the Asian continent, particularly during spring (e.g., Jaffe et al., 1999, 2004, 2005; Kotchenruther et al., 2001; Bertschi et al., 2004; de Gouw et al., 2004; Price et al., 2004; Bertschi and Jaffe, 2005). The mechanisms by which Asian emissions increase O<sub>3</sub> levels over the U.S. west coast are complex and their relative contribution to surface O<sub>3</sub> levels are not fully known. During INTEX-B, the model calculated surface ozone enhancements in the western U.S. attributable to production in the Asian BL (~2–4 ppbv) were comparable to the O<sub>3</sub> produced in the middle and upper troposphere during trans-Pacific transport (~1–4 ppbv) (Zhang et al., 2008, 2009). Decomposition of PAN during air mass subsidence over the eastern Pacific is likely a major driver of O<sub>3</sub> production over the western U.S. in air masses impacted by Asian emissions (Kotchenruther et al., 2001; Jaeglé et al., 2003; Hudman et al., 2004; Zhang et al., 2008, 2009; Fischer et al., 2010a). A recent modeling analysis suggested that the springtime maximum in mid-tropospheric O<sub>3</sub> over the U.S. west coast is largely driven by transport from Asia, coupled with a minimum in O<sub>3</sub> destruction (Brown-Steiner and Hess, submitted for publication).

A major goal of the present work is to identify sources of the highest O<sub>3</sub> levels observed during 2004–2009 at MBO. In Section 2 we describe the MBO research station, the measurements and other tools we used in this analysis. Section 3.1 describes our methods for segregating FT and BL air masses at MBO, while Section 3.2 gives a statistical overview of selected measurements made at MBO during 2004–2009. We describe our definition of high-ozone events in Section 3.3, together with our methodology for characterizing each event and our event type classification scheme. An overview of general features observed during high-ozone events is given in Section 3.4. Section 3.5 provides a detailed case study analysis for each event type. Finally, the results are summarized and conclusions drawn in Section 4.

## 2. Site description, measurements, model and satellite products

### 2.1. Site description

The Mt. Bachelor Observatory is located at the summit of Mt. Bachelor in the Deschutes National Forest in central Oregon, USA (43.98 °N, 121.69 °W, 2763 m asl) (Fig. 1). Owing to its elevation, prevailing westerly winds, the regional topography, and lack of large urban/industrial emissions sources upwind, the observatory

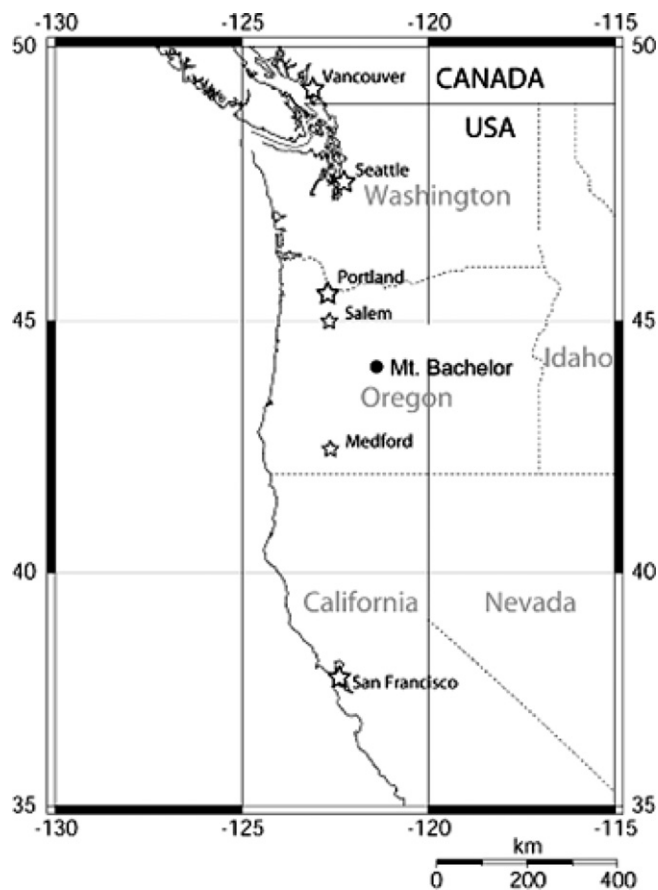


**Fig. 1.** Location of the Mt. Bachelor Observatory (MBO), regional urban areas (Vancouver, British Columbia, Canada; Seattle, Washington; Portland, Oregon; and San Francisco, California) and sounding sites (Medford and Salem, Oregon).

is well positioned for sampling FT air masses with minimal influence from local anthropogenic emissions (Weiss-Penzias et al., 2006). The nearest populated areas are Bend, Oregon (pop. 76,639), 31 km to the east and Redmond, Oregon (pop. 26,215), 53 km northeast.

A suite of chemical and meteorological parameters, including  $O_3$  and CO mixing ratios, Hg mass concentration, sub-micron particle scattering at 530 nm ( $\sigma_{sp}$ ), temperature, pressure, relative humidity (RH), wind speed and direction have been made at MBO near-continuously since February 2004. Instruments are housed in the summit chairlift building of the Mt. Bachelor Ski Area (Fig. 2). The primary sampling inlets extend a few meters above the building roof, which is  $\sim 8$  m above the snow surface, and consist of  $3/8$  inch O.D. Teflon for trace gas sampling and  $3/4$  inch O.D. nonconductive tubing for particle sampling. A separate inlet for Hg is located a few meters below the height of the main sample inlet, on the west side of the building. Since the chairlift itself is electric, the only emissions at the summit are due to the occasional passes of snow-grooming equipment. Contamination from these groomers is easily identified by spikes of CO and  $\sigma_{sp}$ , and these data have been screened out of our analyses.

In the present analysis we focus on observations made from 2004–2009. Most data were collected between March and October when weather conditions at the mountain are most favorable for accessing the summit. During winter (DJF), spring (MAM), summer (JJA) and fall (SON) seasons we measured  $O_3$  during 9462, 12,711, 13,080, and 11,194 h, corresponding with 73%, 96%, 99%, and 85% data coverage for each season, respectively. The measurements are

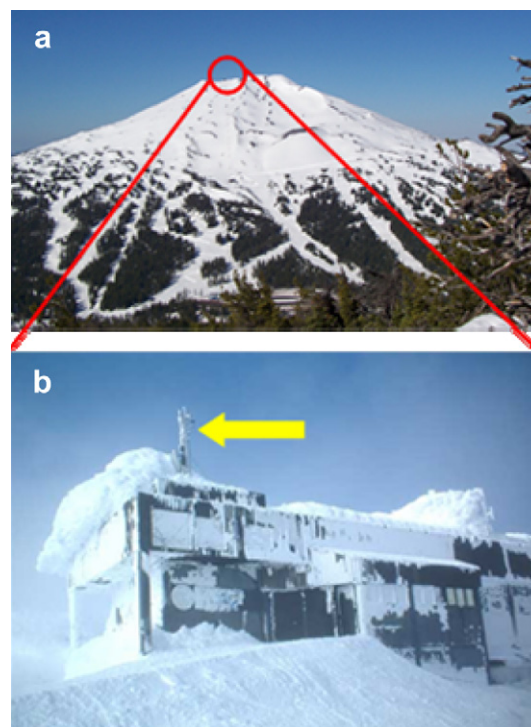


**Fig. 2.** (a) View of the NNE face of Mt. Bachelor with (b) the summit lift building highlighted in red. The yellow arrow in (b) shows the location of the inlet tower (For interpretation of the references to color in this figure legend, the reader is referred to the web version of this article.).

described in detail in Section 2.2 and references therein. All parameters, except Hg (Section 2.2.1), PAN and the  $NO_x$  species (Section 2.2.2), were measured at 20 s temporal resolution and archived as 1–5 min averages. Hourly-averaged values were used here for all parameters except Hg. Times are presented in UTC. For reference, local time at Mt. Bachelor is PST (UTC–8 h) from November to mid-March and PDT (UTC–7 h) at other times.

## 2.2. Measurements

### 2.2.1. Semi-continuous chemical and meteorological measurements

Measurements of  $O_3$  were made by UV photometry using a Dasibi 1008-RS instrument (Weiss-Penzias et al., 2006). The method detection limit (MDL) was 1 ppbv. The total uncertainty was  $\pm 2\%$  for  $O_3 > 5$  ppbv.

Measurements of CO were made by non-dispersive IR absorbance using a TECO 48C CO analyzer during spring of 2004 and a TECO 48C Trace Level Enhanced CO analyzer thereafter (Jaffe et al., 2005; Weiss-Penzias et al., 2006, 2007). The MDL was  $\leq 20$  ppbv. The total uncertainty was  $< \pm 10\%$  at typical ambient levels.

Water vapor (WV) mixing ratios (g/kg) were calculated from measurements of temperature ( $T$ , in units of  $^{\circ}C$ ), relative humidity (RH) and pressure ( $P$ , in units of hPa) following Bolton (1980). Temperature and RH were measured with two Campbell Scientific probes (model HMP 45C). One probe (outside probe) was located near the main sample inlet scaffolding and operated from 2004–2009. A second probe (sheltered probe) was installed beneath an overhang on the east side of the building in 2006 to provide more reliable measurements during the harsh winter and spring months when the sensor atop the roof was susceptible to icing. Pressure was measured with a Vaisala PTB101B transmitter. The accuracies of the  $T$ , RH and  $P$  measurements were estimated to be  $< \pm 0.4$   $^{\circ}C$ ,  $< \pm 5\%$  RH and  $\pm 4$  mbar under the range of

non-condensing conditions encountered at MBO. The outside and sheltered WV values typically agreed to within  $\pm 15\%$  and  $\pm 0.3 \text{ g kg}^{-1}$  when RH was  $< 90\%$ .

Sub-micron aerosol scattering was measured at 530 nm with a Radiance Research M903 nephelometer. The MDL was  $\leq 0.7 \text{ Mm}^{-1}$ . The total uncertainty was  $< \pm 5\%$  for  $\sigma_{\text{sp}} > 2 \text{ Mm}^{-1}$ . Starting in April 2008 the M903 scattering data were supplemented with measurements of sub-micron aerosol scattering made at 450, 550 and 700 nm with a TSI Model 3563 nephelometer (Fischer et al., 2010b). Measurements at 550 nm were used here. The MDL of the TSI nephelometer was  $0.7 \text{ Mm}^{-1}$ . The total uncertainty was  $\pm 8\%$  at  $\sigma_{\text{sp}} = 30 \text{ Mm}^{-1}$ . Here we report all scattering data at STP ( $T = 273.15 \text{ K}$ ,  $P = 1013.25 \text{ hPa}$ ).

Mercury was measured primarily during the spring, summer and fall (typically only through September) seasons. A Tekran 2537A analyzer was used for Hg quantification, with detection by cold vapor atomic fluorescence spectroscopy (CVAFS). From February 2004–March 2005, TAM ( $\equiv \text{GEM} + \text{RGM} + \text{PHg}$ ) was converted to gaseous elemental mercury (GEM) within a custom heated inlet and  $500^\circ \text{C}$  pyrolyzer upstream of the 2537A analyzer (Jaffe et al., 2005; Weiss-Penzias et al., 2006). During March 2005 the pyrolyzer was replaced with a high-volume cyclone inlet system and Tekran 1130 and 1135 samplers to provide TAM speciation, with separate measurement of GEM, RGM and PHg thereafter (Landis et al., 2002; Swartzendruber et al., 2006; Finley et al., 2009). All measurements of GEM were made at 5 min time resolution and archived as 1-hr averages. For the speciated measurements, GEM was measured for the first three of every four hours while RGM and PHg were collected. During the fourth hour, RGM and PHg were quantified without concurrent sample collection. The TAM, RGM and PHg measurements were archived as 3-h averages and were used as such here. All Hg measurements are reported at STP.

The  $1\sigma$  precision of the TAM measurements prior to March 2005 was  $\pm 0.01\text{--}0.05 \text{ ng m}^{-3}$  based on the stability of the internal and external calibrations, which agreed to within  $\pm 6\%$ . The MDL was  $< 0.1 \text{ ng m}^{-3}$ . The total uncertainty was estimated to be  $< \pm 16\%$ .

The  $1\sigma$  precision of the GEM measurements made after March 2005 was  $\pm 0.01\text{--}0.05 \text{ ng m}^{-3}$ . The internal and external calibrations of the 2537A analyzer agreed to within  $\pm 10\%$ . The GEM MDL was  $0.1 \text{ ng m}^{-3}$ , while that for RGM and PHg was  $3\text{--}5 \text{ pg m}^{-3}$ . The total uncertainty of the GEM measurements was estimated to be  $\pm 15\%$ . We note that there is limited quantitative data on the accuracy of Tekran RGM and PHg measurements and no routine calibration method for these species has been reported at this time (Gustin and Jaffe, 2010). Previous field intercomparisons between Tekran 1130/1135/2537A Hg speciation systems demonstrated average precisions for RGM and PHg measurements that ranged between  $\pm 10\text{--}20\%$  and  $\pm 40\text{--}70\%$ , respectively (Lyman and Gustin, 2008, 2009; Peterson and Gustin, 2008).

### 2.2.2. Additional measurements

Several additional trace gases, including  $^{222}\text{Rn}$ , PAN, NO, and  $\text{NO}_2$ , were measured at MBO on a non-routine basis during 2004–2009. We used these measurements when available to support our comparison of the seasonal compositions of FT and BL air masses sampled at MBO (Section 3.2). Radon-222 was measured from September 2004–December 2006 using an instrument designed after Whittlestone and Zahorowski (1998). The MDL was  $\leq 115 \text{ mBq m}^{-3}$ ; the overall uncertainty was  $\leq \pm 20\%$  at levels above the MDL. Peroxyacetyl nitrate was measured at 10 min temporal resolution by gas chromatography with electron capture detection (GC-ECD) from March–October 2008 and from March–May 2009 (Fischer et al., 2010a). The PAN MDL was 15 pptv; the overall uncertainty was  $< \pm 10\%$  at levels above the MDL. Nitrogen oxides were measured at 5 min temporal resolution by  $\text{O}_3$  chemiluminescence

during spring, summer and early fall from April 2007–May 2009 using an instrument manufactured by Air Quality Design, Inc. (Reidmiller et al., 2010). The MDL was estimated to be 4–6 pptv for NO and 8–16 pptv for  $\text{NO}_2$ . The  $1\sigma$  precision for NO was estimated to be  $\pm 2$  pptv at mixing ratios of 5–10 pptv; the  $1\sigma$  precision for  $\text{NO}_2$  was estimated to be  $\pm 8\text{--}6$  pptv at 20–60 pptv.

### 2.2.3. Soundings

Data from twice daily (0 and 12 UTC) National Weather Service (NWS) soundings from Medford, Oregon (MFR,  $42.36^\circ \text{ N}$ ,  $122.86^\circ \text{ W}$ , 405 m asl,  $\sim 200 \text{ km}$  SSW of Mt. Bachelor; <http://weather.uwyo.edu/upperair/sounding.html>) were used to define the regional, seasonally averaged FT WV distributions at a pressure altitude equivalent to MBO. The methodology and results are described in Section 3.1.

## 2.3. Model and satellite products

### 2.3.1. Air mass backward trajectories

Air mass backward trajectories were calculated using the NOAA Hybrid Single-Particle Lagrangian Integrated Trajectory (HYSPPLIT, Version 4) model (Draxler and Hess, 1998; Draxler and Rolph, 2011), driven by meteorological model output from the National Centers for Environmental Prediction (NCEP,  $2.5^\circ \times 2.5^\circ$ ) Reanalysis data for 2004 and from the Global Data Assimilation System (GDAS,  $1^\circ \times 1^\circ$ ) for 2005–2009. Ten-day backward trajectory ensembles were initiated from MBO similar to the method described by Weiss-Penzias et al. (2007). Here, backward trajectories were initialized from a box, approximately centered at the Mt. Bachelor summit, defined by 25 horizontal grid points and 5 altitude levels. A trajectory ensemble was calculated for each of the 3 h centered on the time that the maximum 1-h  $\text{O}_3$  mixing ratio was measured. Thus, for each event, a total of 375 trajectories were calculated. In the NCEP meteorology, the Mt. Bachelor summit is located at  $\sim 1800 \text{ m}$  above model ground level (amgl); therefore trajectory starting altitudes were spaced at 100 m intervals from 1600–2000 m amgl. With GDAS meteorology the Mt. Bachelor summit is located at  $\sim 1500 \text{ m}$  amgl and the trajectory initialization interval ranged from  $\sim 1300\text{--}1700 \text{ m}$  amgl.

### 2.3.2. NAAPS model

For high-ozone events during which  $\sigma_{\text{sp}}$  levels were elevated, results from the Naval Research Laboratory's Navy Aerosol Analysis and Prediction System (NAAPS) global aerosol model (<http://www.nrlmry.navy.mil/aerosol>) were used to help distinguish aerosol type (i.e., dust versus smoke) and the source.

### 2.3.3. FIRMS MODIS products

For high-ozone events during which  $\sigma_{\text{sp}}$  levels were elevated and the NAAPS model suggested the aerosol was composed of smoke, Moderate Resolution Imaging Spectroradiometer (MODIS) satellite-derived active fire counts from the Fire Information for Resource Management System (FIRMS) Web Fire Mapper (Justice et al., 2002; Davies et al., 2009) were used to investigate the potential influence of wildfires.

## 3. Results and discussion

### 3.1. Isolating FT air masses at MBO

We have used several techniques for segregating FT and BL air masses at MBO. Weiss-Penzias et al. (2006) and Fischer et al. (2010a) used the WV mixing ratio to identify FT and BL-influenced air masses. These same studies also used WV calculated from the 0 and 12 UTC NWS soundings from MFR and Salem,

Oregon (SLE, 45.0° N, 123.0° W) to determine a representative altitude for the air masses sampled at MBO. Reidmiller et al. (2010) used chairlift soundings coupled with high-resolution NO<sub>x</sub> data from MBO to determine a time of day when the BL influence began at the mountain summit during spring. However, as shown in Section 3.1.2, using a simple time-of-day criterion is too general and does not account for day-to-day changes in meteorology. A comparison of WV from the MFR and SLE soundings to WV data from Mt. Bachelor showed that the MFR data more closely resembled that from MBO in all seasons. Therefore, in this analysis we use soundings from MFR to compare with WV observations at MBO.

### 3.1.1. Medford sounding analysis

We divided the 2004–2009 MFR sounding data into winter, spring, summer, and fall seasons and tested the 0 UTC (4 pm PST) and 12 UTC (4 am PST) WV datasets to determine if they were statistically different at a similar pressure altitude (i.e., ~730 hPa) as MBO. We determined that the 0 UTC and 12 UTC WV data at ~730 hPa were not statistically different in any season (Table 1). The lack of diurnal variability in WV suggests that the 730 hPa level at MFR is generally representative of the FT (see also Weiss-Penzias et al., 2006). Therefore, we averaged all 0 UTC and 12 UTC WV data at ~730 hPa for each season to obtain seasonally averaged FT WV values. The derived average FT WV values were used to extract similar seasonal FT WV distributions from the MBO data (Section 3.1.2).

### 3.1.2. MBO water vapor analysis

A similar analysis to that presented in Section 3.1.1 was performed on the WV data from MBO (Table 1). Where possible, the hourly-averaged WV measurements from the two T/RH probes (Section 2.2.1) were averaged to provide a mean 0 or 12 UTC WV value. The analysis of WV at MBO shows that, in contrast to WV from the MFR soundings, in all seasons there is a significant difference between 0 and 12 UTC values. This suggests that there is an average diurnal change in air mass type sampled at MBO in all seasons, although the diurnal variation in WV is very small during winter. While a statistically significant diurnal change in meteorological parameters may occur at MBO, the same is not necessarily true for chemical parameters since the BL surrounding MBO is relatively clean, as shown by comparison of NO<sub>x</sub> levels in BL-influenced air measured at MBO and other mid-latitude mountaintop sites in the NH (Reidmiller et al., 2010).

We defined a seasonal FT dataset for WV at MBO by using the seasonal distribution of all WV data at 730 hPa from the MFR soundings. We then extracted a similar distribution in WV data from MBO by retaining the driest portion of the MBO WV distribution such that the seasonal mean WV mixing ratios at MBO and at the 730 hPa level at MFR were equivalent to within 0.01 g kg<sup>-1</sup>. We refer to this dataset as the MBO FT data, which for winter, spring, summer, and fall seasons corresponded with WV <3.28, <3.28, <5.40, and <4.12 g kg<sup>-1</sup>, respectively. We refer to the non-retained dataset as non-FT data.

The hourly frequency distributions for the MBO FT data are illustrated in Fig. 3. During winter, spring, summer, and fall, 78%, 53%, 63%, and 69%, respectively, of MBO data were included in the FT dataset, based on the corresponding WV distributions from the MFR soundings. In all seasons except summer, the majority of FT data were collected at night, which is expected based on the typical diurnal pattern of up-slope (BL-influenced) flows during the day and down-slope (FT-influenced) flows at night. During summer the number of daylight hours (~13–15) is much greater than nighttime hours (~9–11) at the latitude of MBO, resulting in a greater contribution from daytime hours to the FT dataset. In all seasons the fraction of nighttime hours included in the FT dataset was greater than the fraction of daytime hours. The frequency distributions in Fig. 3 argue against previous methods of isolating FT air at MBO based on a simple time-of-day segregation criterion, as was done by Reidmiller et al. (2010).

The strongest diurnal changes in the percentage of hours retained in the FT dataset occurred during summer. This is likely driven, in part, by the fact that the mountain is no longer snow-covered during the warmer summer months. As a result, greater surface heating occurs during summer (as Mt. Bachelor is bare, black volcanic rock above ~2 km asl), allowing for a greater diurnal change between up-slope and down-slope regimes.

## 3.2. Statistical distributions

### 3.2.1. Basic statistics by season

Table 2 compares the seasonal mean distributions of selected chemical and meteorological parameters measured at MBO during 2004–2009. During spring, O<sub>3</sub>, CO, TAM, and PAN reach their annual maxima at MBO. Mixing ratios of CO at northern midlatitudes tend to peak during winter and early spring in part due to reduced photooxidation, coupled with enhanced BB in the NH

**Table 1**  
Statistical results for WV data from the MFR soundings and from Mt. Bachelor from 2004–2009. The results show that in all seasons there is no significant difference between 0 and 12 UTC WV mixing ratios at 730 hPa from the MFR soundings. In contrast the WV data from MBO show a significant difference in all seasons.

Season	Time (UTC)	WV mean (g kg <sup>-1</sup> )	WV variance (g kg <sup>-1</sup> )	Skewness coefficient	F statistic	p-value	Equality of variance?	t statistic	p-value	Equality of means?
<i>MFR sounding data</i>										
DJF	0	2.03	1.50	0.46	0.98	0.41	Yes	-0.41	0.23	Yes
	12	2.13	1.53	0.69						
MAM	0	2.42	1.99	0.18	1.01	0.46	Yes	1.27	0.21	Yes
	12	2.30	1.97	0.50						
JJA	0	3.72	4.30	0.15	1.07	0.24	Yes	1.03	0.30	Yes
	12	3.58	4.02	0.36						
SON	0	2.65	2.58	0.33	1.05	0.30	Yes	1.36	0.17	Yes
	12	2.51	2.45	0.45						
<i>MBO data</i>										
DJF	0	2.63	1.11	0.15	1.10	0.15	Yes	3.66	<0.01	No
	12	2.38	1.01	0.27						
MAM	0	3.78	1.34	0.41	0.95	0.30	Yes	11.90	<0.01	No
	12	2.93	1.19	0.38						
JJA	0	5.84	2.08	0.21	0.62	<0.01	No	19.04	<0.01	No
	12	3.96	3.33	0.09						
SON	0	3.82	1.49	0.15	0.97	0.37	Yes	7.46	<0.01	No
	12	3.07	1.51	0.24						

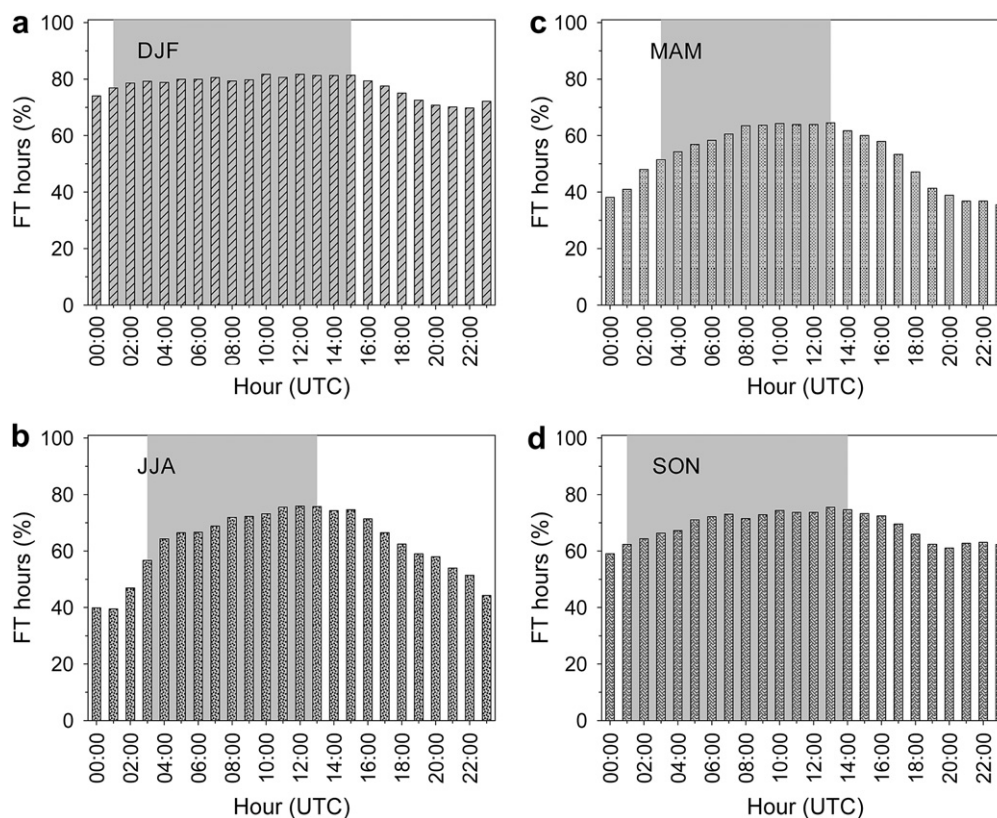


Fig. 3. Hourly frequency of FT WV data at MBO (described in Section 3.1) for (a) winter, (b) spring, (c) summer, and (d) fall. Shading approximately identifies local nighttime hours.

(Novelli et al., 1992; Duncan et al., 2003). Efficient trans-Pacific transport of Asian emissions contributes to elevated springtime baseline CO over the U.S. west coast (Yienger et al., 2000), in addition to episodic enhancements in O<sub>3</sub>, TAM and PAN as observed at MBO (see Weiss-Penzias et al., 2006, 2007; Wolfe et al., 2007; Reidmiller et al., 2009; Fischer et al., 2010a). Mean FT CO, TAM and <sup>222</sup>Rn were all significantly higher than non-FT levels during spring, consistent with a dominant role of ALRT in influencing FT pollutant levels over the U.S. west coast during this time of year. The springtime O<sub>3</sub> maximum is likely significantly influenced by STE (Yienger et al., 2000). We note that in comparison to our measurements at MBO during 2004, the Trinidad Head ozonesonde data from 1997–2004 demonstrate higher mean springtime O<sub>3</sub> at a similar pressure altitude, which is due in part to stronger

subsidence at THD (Weiss-Penzias et al., 2006). During summer, FT CO at MBO reaches a minimum, which coincides with increased photooxidation and less efficient trans-Pacific transport of Asian emissions to the lower FT over the U.S. west coast (Yienger et al., 2000; Liu et al., 2003). Higher and more variable mean  $\sigma_{sp}$  and NO<sub>x</sub> during summer and fall partly reflect a greater influence from regional BB during these seasons.

### 3.3. Classification of high-ozone events at MBO

#### 3.3.1. Definition of high-ozone events

We concentrate on time periods at MBO for which the maximum daily 8-h average O<sub>3</sub> mixing ratio, MDA-8, exceeded 70.0 ppbv, which corresponds with the upper limit value of the

Table 2

Statistical distributions of chemical and meteorological parameters measured at MBO from 2004–2009.

Mean $\pm 1\sigma^a$	DJF		MAM		JJA		SON	
	FT	Non-FT	FT	Non-FT	FT	Non-FT	FT	Non-FT
N <sup>b</sup> (h)	7379	2074	6676	5920	8291	4788	7249	3271
T (°C)	<b>-7.3 <math>\pm</math> 5.2</b>	<b>-2.8 <math>\pm</math> 2.5</b>	<b>-5.9 <math>\pm</math> 5.2</b>	<b>0.6 <math>\pm</math> 4.7</b>	<b>8.3 <math>\pm</math> 6.2</b>	<b>10.5 <math>\pm</math> 5.2</b>	<b>0.5 <math>\pm</math> 7.8</b>	<b>3.8 <math>\pm</math> 5.3</b>
RH (%)	<b>74 <math>\pm</math> 28</b>	<b>93 <math>\pm</math> 11</b>	<b>75 <math>\pm</math> 26</b>	<b>83 <math>\pm</math> 19</b>	<b>43 <math>\pm</math> 25</b>	<b>65 <math>\pm</math> 21</b>	<b>56 <math>\pm</math> 33</b>	<b>80 <math>\pm</math> 23</b>
WV (g kg <sup>-1</sup> )	<b>2.1 <math>\pm</math> 0.6</b>	<b>3.9 <math>\pm</math> 0.3</b>	<b>2.4 <math>\pm</math> 0.6</b>	<b>4.4 <math>\pm</math> 0.8</b>	<b>3.6 <math>\pm</math> 1.3</b>	<b>6.6 <math>\pm</math> 0.9</b>	<b>2.6 <math>\pm</math> 1.0</b>	<b>5.1 <math>\pm</math> 0.8</b>
O <sub>3</sub> (ppbv)	<b>43 <math>\pm</math> 7</b>	<b>39 <math>\pm</math> 6</b>	<b>50 <math>\pm</math> 9</b>	<b>44 <math>\pm</math> 8</b>	<b>46 <math>\pm</math> 11</b>	<b>39 <math>\pm</math> 11</b>	<b>42 <math>\pm</math> 10</b>	<b>34 <math>\pm</math> 8</b>
CO (ppbv)	<b>125 <math>\pm</math> 19</b>	<b>118 <math>\pm</math> 20</b>	<b>149 <math>\pm</math> 24</b>	<b>141 <math>\pm</math> 23</b>	<b>111 <math>\pm</math> 32</b>	<b>118 <math>\pm</math> 40</b>	<b>115 <math>\pm</math> 83</b>	<b>107 <math>\pm</math> 62</b>
$\sigma_{sp}$ (Mm <sup>-1</sup> )	<b>0.8 <math>\pm</math> 1.3</b>	<b>0.5 <math>\pm</math> 1.4</b>	<b>3.5 <math>\pm</math> 5.7</b>	<b>5.0 <math>\pm</math> 5.7</b>	<b>9.8 <math>\pm</math> 23.4</b>	<b>18.3 <math>\pm</math> 30.0</b>	6.3 $\pm$ 35.9	7.4 $\pm$ 36.0
TAM (ng m <sup>-3</sup> )	<b>1.51 <math>\pm</math> 0.11</b>	<b>1.42 <math>\pm</math> 0.15</b>	<b>1.70 <math>\pm</math> 0.17</b>	<b>1.65 <math>\pm</math> 0.15</b>	<b>1.50 <math>\pm</math> 0.11</b>	<b>1.46 <math>\pm</math> 0.12</b>	<b>1.46 <math>\pm</math> 0.10</b>	<b>1.45 <math>\pm</math> 0.13</b>
<sup>222</sup> Rn (mBq m <sup>-3</sup> ) <sup>c</sup>	<b>533 <math>\pm</math> 301</b>	<b>474 <math>\pm</math> 253</b>	<b>702 <math>\pm</math> 619</b>	<b>572 <math>\pm</math> 469</b>	<b>335 <math>\pm</math> 137</b>	<b>462 <math>\pm</math> 167</b>	<b>551 <math>\pm</math> 593</b>	<b>805 <math>\pm</math> 1053</b>
NO <sub>x</sub> (pptv) <sup>c</sup>	<sup>d</sup>	<sup>d</sup>	<b>108 <math>\pm</math> 79</b>	<b>114 <math>\pm</math> 62</b>	<b>96 <math>\pm</math> 45</b>	<b>158 <math>\pm</math> 68</b>	<b>121 <math>\pm</math> 84</b>	<b>261 <math>\pm</math> 840</b>
PAN (pptv) <sup>c</sup>	<sup>d</sup>	<sup>d</sup>	<b>149 <math>\pm</math> 84</b>	<b>115 <math>\pm</math> 83</b>	<b>91 <math>\pm</math> 43</b>	<b>69 <math>\pm</math> 29</b>	<b>107 <math>\pm</math> 132</b>	<b>93 <math>\pm</math> 53</b>

<sup>a</sup> Bold type indicates FT and non-FT values are significantly different ( $p < 0.05$ ).

<sup>b</sup> Number of hours during which O<sub>3</sub> was measured.

<sup>c</sup> Non-routine measurements.

<sup>d</sup> Not measured.

anticipated revised NAAQS (EPA, 2010). We note that the EPA O<sub>3</sub> NAAQS is defined at a higher tolerance (i.e., 1 ppbv unit) than used here to classify high ozone events at MBO. (Hereinafter, time periods during which MDA-8 exceeded 70.0 ppbv are referred to as high-ozone events.) We defined event duration as the number of hours with O<sub>3</sub> > 70.0 ppbv. A total of 25 high-ozone events were recorded from 2004–2009, with a total duration of 221 h.

### 3.3.2. Methodology for high-ozone event characterization; source type classification scheme

For each event, we conducted a linear least squares regression analysis for (i) O<sub>3</sub>, TAM and  $\sigma_{sp}$  versus CO and (ii) O<sub>3</sub> versus WV using measurements from the 24-hour period centered on the time when the maximum 1-h O<sub>3</sub> mixing ratio was recorded. Additionally, for each event we compared the values of chemical and meteorological variables for the hours with O<sub>3</sub> > 70.0 ppbv with the distribution during the month in which the event occurred. Levels of chemical and meteorological variables during each event will be referred to in the following discussion as either depleted or enhanced relative to the corresponding monthly median values as summarized in Table 3. Likewise, correlation slopes will be referred to as strong, weak or not statistically significant (i.e., no correlation) as summarized in Table 4. Finally, air mass backward trajectories (Section 2.3.1), results from the NAAPS model (Section 2.3.2) and FIRMS MODIS products (Section 2.3.3) were used to support our identifications.

The high-ozone event source classification scheme developed through this analysis is summarized in Table 5. An attempt was not made to identify sources for events during which either (1) CO was not measured or (2) both  $\sigma_{sp}$  and TAM were not measured.

Fig. 4 compares the values of several key chemical parameters, including the average event-mean percentile ranks for CO and TAM and the average O<sub>3</sub>/CO correlation slopes for each event type. Among the measured and derived chemical parameters, these showed the most significant differences between events of each type, as discussed below. Fig. 5 compares each type of classifiable high-ozone event in terms of total number and duration.

### 3.4. High-ozone event general features

High-ozone events were identified in spring, summer and fall seasons, with the greatest number occurring in spring and summer (Table S1). Event frequency and duration were highest in 2009 and lowest in 2004. For all years, our O<sub>3</sub> data coverage was >90% during spring, summer and fall seasons, with the exception of fall 2005 when it was 33%. These overall minor differences in sample collection suggest that the observed seasonal and inter-annual variability in high-ozone event frequency and duration resulted from real variability in the underlying sources and were not biased by sample collection.

**Table 3**  
Classification scheme for chemical parameters measured at MBO from 2004–2009.

Percentile rank <sup>a</sup>	Classification
<10th	Strongly depleted
<25th and ≥10th	Depleted
<40th and ≥25th	Moderately depleted
40th–60th	Central 20%
>60th and ≤75th	Moderately enhanced
>75th and ≤90th	Enhanced
>90th	Strongly enhanced

<sup>a</sup> Determined for the mean value of each parameter measured during time periods with O<sub>3</sub> > 70.0 ppbv.

**Table 4**  
Classification scheme for correlations between parameters measured at MBO from 2004–2009.

$r^{2a}$	$p$ -value	Classification
<0.50	≥0.15	No correlation <sup>b</sup>
<0.50	<0.15	Very weak
<0.50	<0.05	Weak
>0.50	<0.05	Moderate
>0.75	<0.05	Strong
>0.90	<0.05	Very strong

<sup>a</sup> Determined for the 24-h period centered on the time that the maximum 1-h O<sub>3</sub> mixing ratio was recorded for each high-ozone event.

<sup>b</sup> Abbreviated as NC in Table S1.

Table S1 summarizes the chemical characteristics of all high-ozone events observed at MBO during 2004–2009. For several of the events, the corresponding time periods were analyzed in detail in previous work, and the event-type classifications were taken partly from the referenced studies. We note that most of the high-ozone events identified here were not identified previously.

As demonstrated in Table S1, a general feature of all the high-ozone events observed at MBO was that the associated WV mixing ratios were depleted (usually strongly) relative to the corresponding monthly median values, with all event hours being included in the MBO FT dataset as defined in Section 3.1.2. Additionally, the O<sub>3</sub> and WV mixing ratios were anti-correlated during all events with O<sub>3</sub>/WV correlation slopes ranging from  $-5.0 \pm 0.5$  to  $-23.3 \pm 1.6$  ppbv g<sup>-1</sup> kg<sup>-1</sup>. Furthermore, nearly all high-ozone periods occurred during nighttime. These features are consistent with a dominant influence from FT air masses (Weiss-Penzias et al., 2006, 2007; Reidmiller et al., 2010). In contrast, NABB (PNW) and NAI sources are typically characterized by a relatively high degree of BL transport and reach MBO with elevated WV mixing ratios (Weiss-Penzias et al., 2007; Finley et al., 2009); these sources likely made minimal contributions to the O<sub>3</sub> enhancements measured during the high-ozone events listed in Table S1. For reference, supplemental sections S1 and S2 provide further details on characteristics of NABB and NAI-influenced air masses observed at MBO.

**Table 5**  
High-ozone event classification scheme.

Event type <sup>a</sup>	Characteristic features <sup>b</sup>	No. events at MBO
UT/LS	"Key indicators" <sup>c</sup> : CO < 25th percentile; TAM < 10th percentile; O <sub>3</sub> /CO slope < 0 ( $p < 0.05$ ) Other indicators: CO < 40th percentile; TAM < 40th percentile; WV < 25th percentile; O <sub>3</sub> /CO slope ≤ 0	8
ALRT	"Key indicators": CO > 90th percentile; TAM > 90th percentile; TAM/CO slope = $5 \pm 1 \times 10^{-3}$ ( $p < 0.05$ ) Other indicators: CO > 60th percentile; WV < 25th percentile; O <sub>3</sub> /CO slope ≥ 0; $\sigma_{sp}$ /CO slope ≥ 0	4
ALRT + UT/LS	"Key indicators": CO ≥ 10th percentile, ≤75th percentile; TAM > 60th percentile, ≤75th percentile; TAM/CO slope = $5 \pm 1 \times 10^{-3}$ ( $p < 0.05$ ); $\sigma_{sp}$ /CO slope > 0 ( $p < 0.05$ ) Other indicators: WV < 25th percentile; $\sigma_{sp} > 50$ th percentile	6
ND	No CO data; trajectories ambiguous	7

<sup>a</sup> ALRT, Asian long range transport; UT/LS, upper troposphere/lower stratosphere; ND, not determined.

<sup>b</sup> Units: O<sub>3</sub>/CO slope, ppbv ppbv<sup>-1</sup>; TAM/CO slope, ng m<sup>-3</sup> ppbv<sup>-1</sup>;  $\sigma_{sp}$ /CO slope, Mm<sup>-1</sup> ppbv<sup>-1</sup>.

<sup>c</sup> High confidence was only assigned to identifications for which "at least two of the 'key indicators' were satisfied"; additionally, it was necessary that the 10-day backward trajectory ensembles were consistent with the measurement-based source assignments.

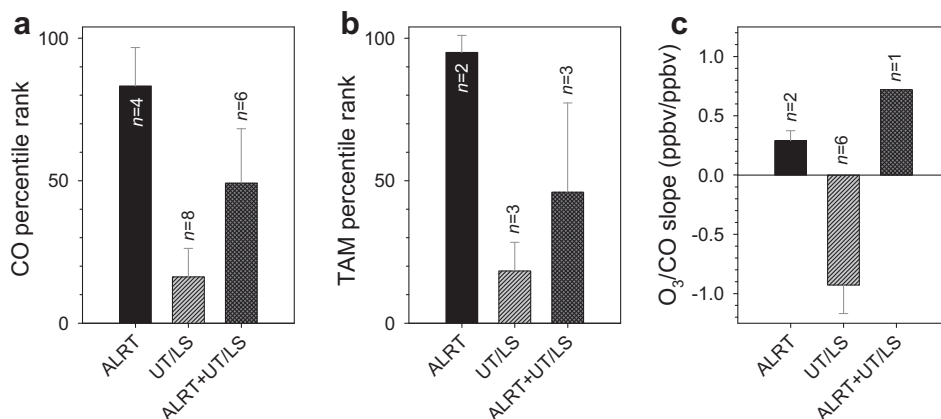


**Fig. 4.** Comparison between the relative levels of (a) CO and (b) TAM measured during the high-ozone events observed at MBO during 2004–2009. The average ( $\pm 1\sigma$ ) percentile ranks of the event-mean CO mixing ratios and TAM mass concentrations are shown for each event type. All classifiable events are represented in (a), while only the subset of events for which TAM measurements were available is represented in (b). The average  $O_3/CO$  correlation slopes calculated for the high-ozone events are compared for each event type in (c); error bars represent  $\pm 1\sigma$  and only values for events with statistically significant correlations ( $p \leq 0.05$ ) were considered (Table S1).

While regional BB events in summer and fall are relatively common (e.g., Weiss-Penzias et al., 2007), none of these events in 2004–2009 had 8-h averaged  $O_3 > 70.0$  ppbv. In contrast, PNW fires in summer 2010 resulted in at least one high-ozone event as defined here. The 2010 data will be presented separately (Wigder et al., in preparation).

An additional feature common to all high-ozone events was that the air mass backward trajectory ensembles suggested varying degrees of trans-Pacific transport and influence from the western Pacific region. Consistent with the WV analysis, the trajectory results suggest minimal influence from surface emissions over North America, further ruling out strong contributions from NAI and NABB (PNW and Alaska) sources. We note that the frequency of each event type determined in our analysis depends in part on the “threshold”  $O_3$  mixing ratio chosen for the high-ozone event definition, as was described previously regarding analyses of the influence of stratospheric intrusions on surface  $O_3$  levels (c.f., Stohl et al., 2000). Although they did not contribute to enhanced  $O_3$  during the high-ozone events identified here (i.e., MDA-8  $> 70.0$  ppbv), U.S. emissions, particularly NABB, clearly contribute to smaller  $O_3$  enhancements observed at MBO (e.g., Weiss-Penzias et al., 2007).

Ozone production from BB emissions, although it is not well understood, is expected to depend significantly on (1) combustion conditions (i.e., flaming versus smoldering), which influences the emissions spectrum as well as the vertical distribution of emissions,

and (2) the transport path from source to receptor (i.e., BL versus FT transport) (e.g., Val Martín et al., 2006; Tanimoto et al., 2008). Loss of  $O_3$  due to dry deposition during BL transport as well as lower baseline  $O_3$  levels in the BL than in the FT may partly explain why no PNW BB high-ozone events were identified in our analysis. However, further work is required to better understand factors governing  $O_3$  production from NABB emissions observed at MBO.

### 3.5. High-ozone event case study examples

#### 3.5.1. Upper-troposphere/lower-stratosphere (UT/LS) events

Subsidence of dry, ozone-rich air masses from the upper troposphere/lower stratosphere has been suggested as an influence on atmospheric composition at MBO in several previous studies (Swartzendruber et al., 2006; Weiss-Penzias et al., 2006; Wolfe et al., 2007; Adhikary et al., 2010). However, the UT/LS influence type has not been fully characterized in terms of its climatology and relative importance for enhancing  $O_3$  mixing ratios.

The probability that a high-ozone event at MBO was influenced by stratospheric  $O_3$  corresponds with the altitude profile and horizontal distribution of the associated backward trajectories. Trajectories that attained pressure altitudes closer to tropopause pressure (TPP) in regions with higher STE fluxes had a greater probability of entraining stratospheric  $O_3$ . For June and December 2005, the mean  $\pm 1\sigma$  extra-tropical TPP was calculated to be  $228 \pm 47$  hPa and  $235 \pm 50$  hPa, respectively (Tang and Prather, 2010). The tropopause height at northern mid-latitudes ranges from  $\sim 10$  km during winter–spring to  $\sim 12$  km during fall (e.g., Kentarchos and Roelofs, 2003; Newchurch et al., 2003).

The 22 April 2006 high-ozone event (Fig. 6(a–d)) was discussed previously (Wolfe et al., 2007; Adhikary et al., 2010). Although TAM measurements were not made on 22 April, measurements of CO suggest a relatively unpolluted air mass was sampled (Table S1). For instance CO was depleted, with the event-mean mixing ratio being  $< 22$ nd percentile value for April. Mixing ratios of PAN measured via chemical ionization-mass spectrometry (CIMS) were not elevated. Furthermore, an analysis of backward trajectories suggested minimal ALRT influence (Wolfe et al., 2007). As described by Wolfe et al. (2007), the lack of concurrent enhancements in other pollutants suggests that the elevated  $O_3$  levels observed on 22 April were driven by subsidence of an  $O_3$ -rich UT/LS air mass. The mean  $O_3$  mixing ratio during the event was  $79.9 \pm 4.9$  ppbv, which corresponded with a 30.2 ppbv enhancement above the 49.7 ppbv

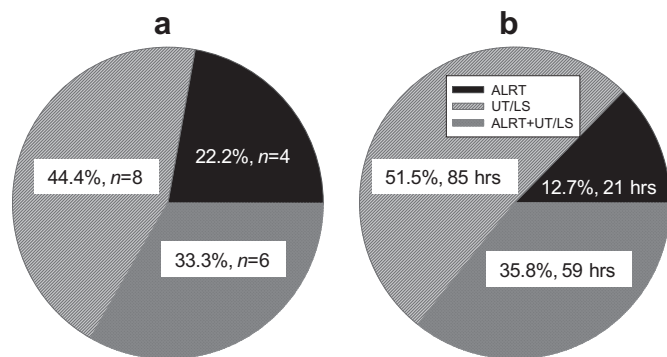


**Fig. 5.** Distribution of each type of high-ozone event observed at MBO from 2004–2009 in terms of (a) number of events ( $n$ ) and (b) number of hours with  $O_3 > 70.0$  ppbv. Only the 18 classifiable events are represented.

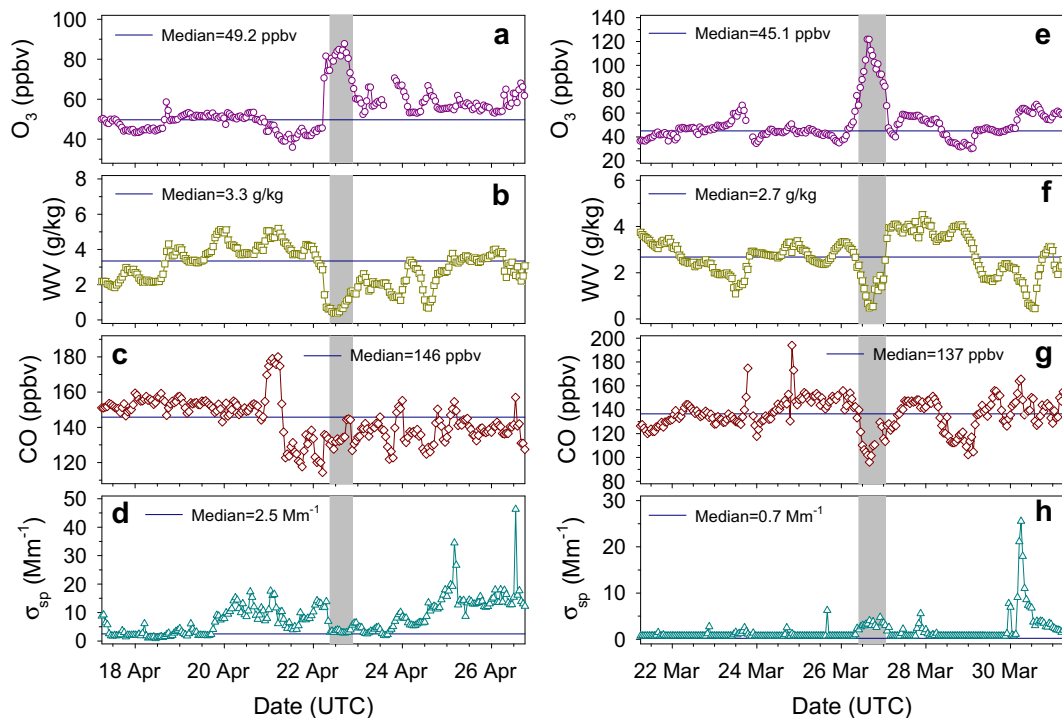


**Fig. 6.** Left panels: Time-series plots of (a)  $O_3$ , (b) WV, (c) CO, and (d)  $\sigma_{sp}$  measured during a 10-day period centered on the 22 April 2006 UT/LS high-ozone event. The monthly median value for each parameter is shown for comparison to levels measured during the event. Right panels (e–h): Same as the left panels except centered on the 26 March 2009 UT/LS high-ozone event. Values of  $\sigma_{sp}$  below the MDL ( $0.7 \text{ Mm}^{-1}$ ) were set to the MDL. Note the different y-axis scales between the left and right panels. Shading indicates the time period with 8-h averaged  $O_3 > 70.0 \text{ ppbv}$ .

monthly median. Model calculations suggest that Asian anthropogenic emissions contributed  $< 10 \text{ ppbv}$  of the total  $O_3$  measured at MBO (Zhang et al., 2008). Therefore, it can be estimated that ALRT accounted for  $< 30\%$  of the measured  $O_3$  enhancement. Results of a more recent modeling study further support a dominant stratospheric influence for the 22 April  $O_3$  enhancement (Adhikary et al., 2010). We note that measurements from the Tropospheric Emission Spectrometer (TES) on board the NASA Aura satellite appear to have captured a regional FT  $O_3$  enhancement coincident with the 22 April high-ozone event observed at MBO (Fig. S1). The same event may have contributed to significantly elevated surface  $O_3$  at CASTNet sites in the Western U.S. (McDonald-Buller et al., submitted for publication).

The 26 March 2009 high-ozone event was not discussed in any previous analyses. Lasting for 16 h with a peak 1-h  $O_3$  mixing ratio of  $121 \pm 2 \text{ ppbv}$ , the 26 March event was one of the longest in duration and had the highest peak  $O_3$  mixing ratio of all the recorded high-ozone events (Table S1; Fig. 6(e–h)). Although Hg

was not measured during the event, CO was strongly depleted, with the event-mean mixing ratio being  $< 4\text{th}$  percentile value for March. While the NAAPS model indicated that MBO was impacted by a descending dust layer, the apparent enhancement in  $\sigma_{sp}$  during the event (Table S1) was not large; the monthly median  $\sigma_{sp}$  was  $0.7 \text{ Mm}^{-1}$  as a result of significant aerosol scavenging during frequent cloudy conditions in the region (i.e., monthly median RH  $> 90\%$  at MBO). Both  $O_3$  and  $\sigma_{sp}$  were anti-correlated with CO with least squares regression slopes of  $-1.3 \pm 0.1 \text{ ppbv ppbv}^{-1}$  ( $r^2 = 0.83$ ,  $p < 0.05$ ) and  $-0.06 \pm 0.01 \text{ Mm}^{-1} \text{ ppbv}^{-1}$  ( $r^2 = 0.56$ ,  $p < 0.05$ ). Air mass backward trajectories (Fig. 7), although highly diffuse, are consistent with a primary influence from the UT/LS region and rapid subsidence on final approach to MBO. The air mass appeared to subside primarily over the eastern Pacific, with the trajectories descending  $> 5 \text{ km}$  during the final 48 h on approach to MBO. The median 10-day transport altitude was  $6.3 \text{ km amgl}$ , corresponding with a median pressure of  $410 \text{ hPa}$ . By comparison, the 10-day median transport altitudes for the 25 April 2004 and 12 May

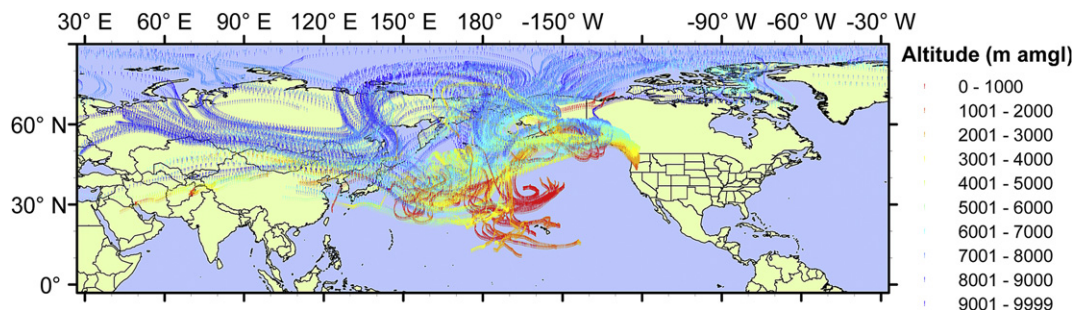


**Fig. 7.** Ten-day air mass backward trajectory ensemble for the 26 March 2009 UT/LS high-ozone event.

2008 ALRT events were 2.6 and 2.1 km amgl, respectively (Section 3.5.2).

In general, UT/LS events were characterized by depleted levels of CO and TAM in comparison to the corresponding monthly median values (Table S1, Fig. 4). Levels of  $\sigma_{sp}$  were typically near the corresponding monthly median values; however, enhancements in  $\sigma_{sp}$  were measured during several events in 2009 (e.g., 16 May, 2009; Table S1). For all of the latter events the NAAPS model suggested an influence from dust aerosol at MBO. (We note that Fischer et al. (2010b) determined that enhanced aerosol loading at MBO on 16 May 2009 was of Asian origin; however, we find no evidence for a significant influence from urban/industrial or BB emissions during the 16 May 2009 high-ozone event (Table S1).) The levels of O<sub>3</sub> and CO tended to be anti-correlated (Fig. 4), whereas no consistent  $\sigma_{sp}$ /CO relationship was observed. Anti-correlation between O<sub>3</sub> and CO is a general feature of UT/LS-influenced air masses (e.g., Stohl et al., 2000; Hoor et al., 2002; Tilmes et al., 2010) and was observed during a stratospheric intrusion event in the lower FT over the southwestern U.S. during the 2006 Tex-AQS/GoMACCS experiment (Brioude et al., 2007). Air mass backward trajectories for the UT/LS events were consistent with significant transport at high altitudes and minimal continental influence within the 10-day period prior to reaching MBO. The UT/LS events occurred during spring and summer and were typically the longest in duration of all recorded events.

### 3.5.2. Asian long range transport (ALRT) events

Asian long range transport consists of transported pollutants from urban/industrial regions in eastern Asia, BB in southeast Asia and/or boreal forest fires in northeastern Russia to the U.S. west coast (e.g., NRC, 2010). Surface emissions are lofted from the Asian BL into the FT by convective, frontal and orographic lifting (Bey et al., 2001; Liu et al., 2003; Cooper et al., 2004a; Liang et al., 2005; Lin et al., 2010). Frontal lifting is the primary mechanism for delivering eastern Asian urban/industrial emissions to the FT (Liu et al., 2003). Once in the FT, pollutants can be efficiently transported eastward toward North America in prevailing westerly winds. Trans-Pacific transport times in the FT are on the order of 4–10 days (Stohl et al., 2002). Subsidence downwind over the northeast Pacific delivers air masses bearing Asian emissions to the lower FT over the U.S. west coast. The influence of ALRT on atmospheric composition over the northeast Pacific is known to be episodic in nature and strongest in springtime, due to more intense frontal activity, and therefore more efficient eastward export of Asian emissions, coupled with a strong easterly jet over the central Pacific (Yienger et al., 2000; Liu et al., 2003).

Aircraft measurements downwind of the Asian continent over the western North Pacific and surface measurements at Hedo Station on Okinawa, Japan identified an Asian urban/industrial GEM/CO ER of 0.0056 ng m<sup>-3</sup> ppbv<sup>-1</sup> (Friedli et al., 2004; Jaffe et al., 2005). Subsequent determinations of the GEM/CO and TAM/CO ERs at MBO were in close agreement with the Asian ER for polluted air masses that could be traced to the Asian continent (Jaffe et al., 2005; Weiss-Penzias et al., 2006, 2007). Long-term Hg measurements from spring 2006 to winter 2007 at the LABS station in Taiwan were also consistent with a springtime Asian GEM/CO ER of 0.005 ng m<sup>-3</sup> ppbv<sup>-1</sup> (Sheu et al., 2010). At MBO, time periods with a strong ALRT influence typically coincided with elevated levels of TAM, CO and  $\sigma_{sp}$ , similar to observations from other analyses of trans-Pacific transport of Asian emissions to the U.S. west coast (e.g., de Gouw et al., 2004; Price et al., 2004; Bertschi et al., 2004; Bertschi and Jaffe, 2005). Long-range transport of Asian anthropogenic emissions to the U.S. west coast was primarily observed during springtime (e.g., Bertschi et al., 2004; Weiss-Penzias et al., 2007), whereas eastern Siberia BB emissions were observed over

the U.S. west coast during spring and summer (Bertschi et al., 2004; Bertschi and Jaffe, 2005).

The 25 April 2004 high-ozone event corresponded with a well-documented case of ALRT observed at MBO (Jaffe et al., 2005; Weiss-Penzias et al., 2006, 2007; NRC, 2010). Levels of CO, TAM and  $\sigma_{sp}$  were strongly enhanced, with mean values during the event that were all >99th percentile values for April (Table S1). Ozone, TAM and  $\sigma_{sp}$  were all strongly correlated with CO during this event, with least squares regression slopes of  $0.23 \pm 0.02$  ppbv ppbv<sup>-1</sup> ( $r^2 = 0.79$ ,  $p < 0.05$ ),  $0.0043 \pm 0.0003$  ng m<sup>-3</sup> ppbv<sup>-1</sup> ( $r^2 = 0.90$ ,  $p < 0.05$ ) and  $0.49 \pm 0.02$  Mm<sup>-1</sup> ppbv<sup>-1</sup> ( $r^2 = 0.95$ ,  $p < 0.05$ ). (We note that small differences between the correlation parameters given here and those reported previously are due to differences in the specific time periods considered.) These relationships are consistent with an influence of urban/industrial emissions on atmospheric composition (including O<sub>3</sub> levels) measured at MBO (Jaffe et al., 2005; Weiss-Penzias et al., 2006, 2007). Air mass backward trajectories for this event were presented previously (Jaffe et al., 2005; Weiss-Penzias et al., 2006).

The 12 May 2008 high ozone event also corresponded with a period of ALRT influence reported previously (Fischer et al., 2010a). The event was characterized by enhanced levels of CO, TAM and  $\sigma_{sp}$ , as for the 25 April 2004 event (Table S1) (Fig. 8(a–d)). Peroxyacetyl nitrate mixing ratios measured by GC-ECD were also enhanced (Fischer et al., 2010a). The event mean CO mixing ratio, TAM mass concentration, and  $\sigma_{sp}$  were all >88th percentile values for May. Although O<sub>3</sub> was not correlated with CO it was strongly correlated with PAN (Table S1), which is consistent with a strong coupling between PAN chemistry and O<sub>3</sub> production associate with the measured O<sub>3</sub> enhancement. The NAAPS model suggests the measured aerosols were transported from Asia. On the basis of air mass backward trajectories associate with this event as well as active fire data for eastern Asia, a mix of Asian urban/industrial and BB emissions likely influenced the elevated levels of pollutants, including O<sub>3</sub>, measured at MBO (Fischer et al., 2010a).

In general ALRT high-ozone events were characterized by levels of CO and TAM that were enhanced (often strongly) compared to the corresponding monthly median values (Table S1, Fig. 4). Levels of O<sub>3</sub>, TAM and  $\sigma_{sp}$  were correlated with CO for some of the ALRT events. These events were likely driven mostly by Asian urban/industrial emissions, as verified by the associated TAM/CO correlation plot slopes. However, as discussed by Fischer et al. (2010a) for the 12 May 2008 event, BB could also be important for governing O<sub>3</sub> levels downwind. The air mass backward trajectories typically extended into the east Asian outflow region (c.f., Bey et al., 2001; Liu et al., 2003) through a zonal plane at 140 °E longitude, extending between ~20–50 °N latitude at an altitude range of ~2–6 km amgl. This transport pattern is consistent with a dominant influence from urban/industrial regions in eastern Asia based on previous model analyses of Asian emissions export to the western Pacific FT (Bey et al., 2001; Liu et al., 2003). The ALRT events typically occurred during springtime and tended to be relatively short in duration.

### 3.5.3. Mixed ALRT + UT/LS events

The important role of STE in influencing the composition of air masses transported across the Pacific to the U.S. west coast was demonstrated previously (Jaeglé et al., 2003; Cooper et al., 2004a,b). Both STE and ALRT (Section 3.5.2) were shown to be strongly associated with mid-latitude cyclonic activity (e.g., Liu et al., 2003; Cooper et al., 2004a). Therefore, it is likely that most trans-Pacific transport corresponds with some degree of UT/LS influence, suggesting that ALRT and UT/LS influences at MBO may often be closely coupled. The mixing of O<sub>3</sub>-rich UT/LS air masses with polluted air masses lofted from the Asian BL could explain exceptionally large O<sub>3</sub>/CO ERs derived from measurements made

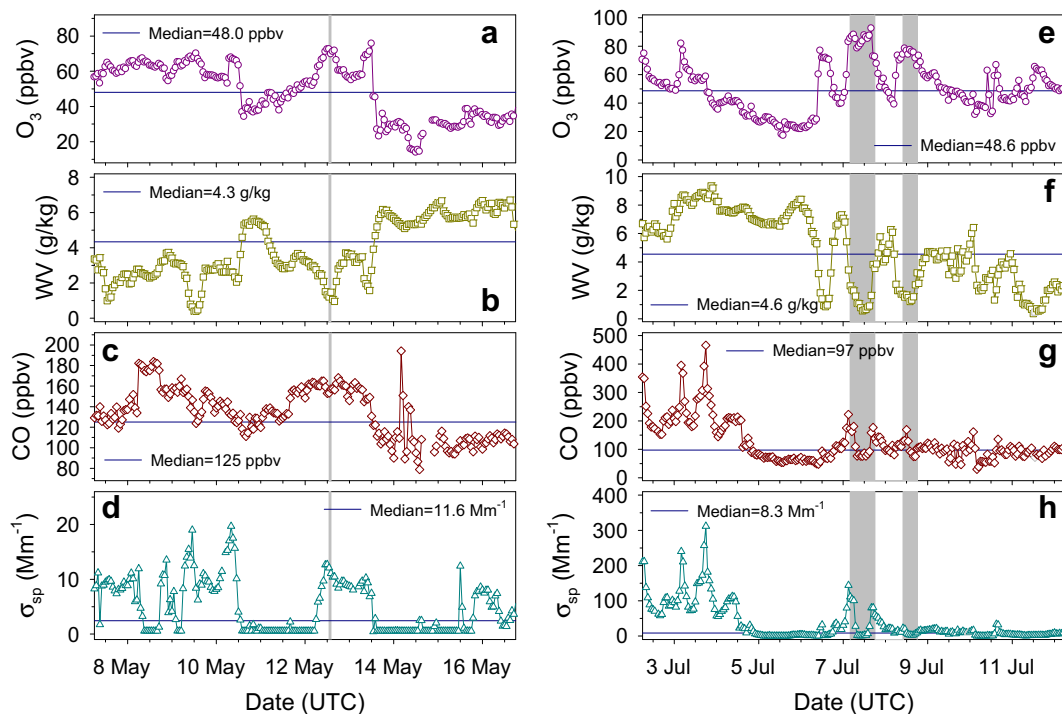


**Fig. 8.** Same as Fig. 6 but for the 12 May 2008 ALRT (a–d) and 7 July 2008 ALRT + UT/LS (e–h) high-ozone events. Scattering data in (d) are from the TSI nephelometer. Note the different scaling of the y-axes for each event. The time period with 8-h averaged  $O_3 > 70.0$  ppbv for the 8 July 2008 high-ozone event is also highlighted in (e–h).

over the eastern Pacific during springtime trans-Pacific transport events in 2001 and 2002 (Price et al., 2004).

The 7 July 2008 high-ozone event exhibited the highest peak 1-h  $O_3$  mixing ratio ( $92 \pm 2$  ppbv) and the longest duration (16 h) of all the mixed ALRT + UT/LS events (Table S1; Fig. 8(e–h)). We therefore describe this event in more detail here. The mean CO mixing ratio during the 7 July event was >71st percentile value for July, but had a 40% relative standard deviation (RSD) as a result of large enhancements at the beginning and end of the event, separated by a longer period with mixing ratios below the monthly median (Fig. 8g). The event-median CO mixing ratio was within the

central 20% of the distribution for July and was therefore intermediate between enhanced levels typical of ALRT events and depleted levels typical of UT/LS events. Although Hg was not measured,  $\sigma_{sp}$  was elevated, though also with large RSD. While  $O_3$  and CO were not correlated,  $\sigma_{sp}$  and CO were strongly correlated with a least squares regression slope of  $0.98 \pm 0.07 \text{ Mm}^{-1} \text{ ppbv}^{-1}$  ( $r^2 = 0.90$ ,  $p < 0.05$ ). The  $\sigma_{sp}$ /CO correlation slope was similar to values reported previously in wildfire smoke plumes transported to the U.S. west coast from eastern Siberia (Bertschi and Jaffe, 2005). The NAAPS model suggests that MBO was influenced by a descending layer of smoke during the event, consistent with long-

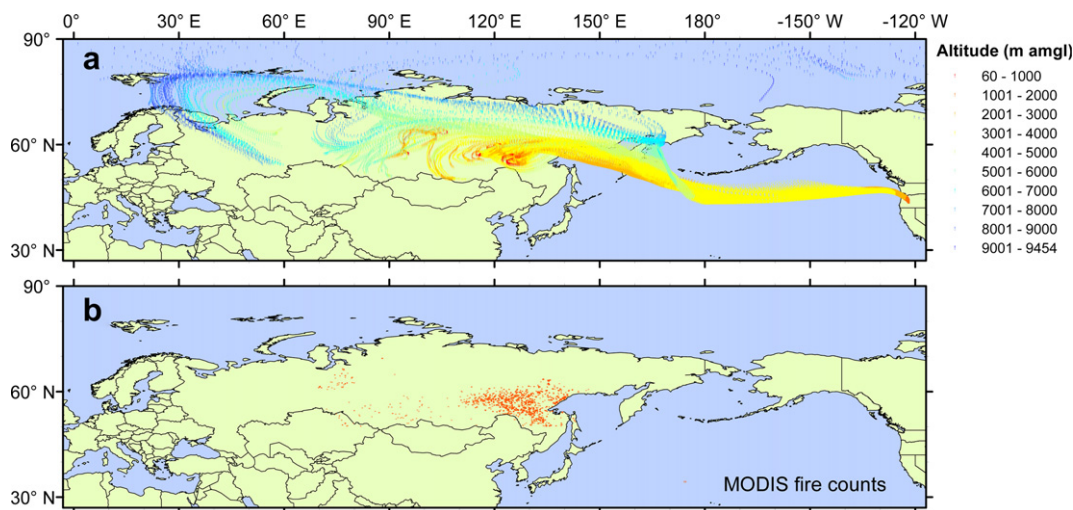


**Fig. 9.** (a) Ten day air mass backward trajectory ensemble for the 7 July 2008 ALRT + UT/LS high-ozone event. (b) Locations of nominal to high-confidence active fire detections from the FIRMS MODIS database for the region encompassed by 50–80°N latitude and 60–180°E longitude and for the time period from 28 June–2 July during which trajectories in (a) made landfall over the Asian continent. Each point in (b) represents the center of a  $\sim 1 \text{ km}^2$  pixel in which at least one active fire was detected.

range transport of wildfire emissions (Fig. S2). The air mass backward trajectories are consistent with an influence from a deep atmospheric column extending from near the surface to  $\sim 9.0$  km aagl over eastern Siberia (Fig. 9a). The MODIS active fire counts for the time period 5–10 days prior to the 7 July event confirm intense BB in eastern Siberia in the region of influence suggested by the trajectory analysis (Fig. 9b). We note that while Fig. 9a shows trajectories only for a time period at the end of the event (15:00–17:00 UTC), trajectories initialized at all other times during the event showed consistent transport. Though they appeared to be associated, our analysis does not conclusively attribute the 7 and 8 July 2008 high-ozone events to the same source. An analysis based on the Sulfur Transport and Deposition Model (STEM) regional chemical transport model suggests a complex plume structure with influence from both Asian BB emissions as well as STE on the O<sub>3</sub> enhancements observed at MBO on 7 and 8 July (Huang et al., submitted for publication).

We note that characteristics of the 28 April 2007 ALRT + UT/LS high-ozone event (Table S1) provide evidence for the confluence of Asian urban/industrial emissions and O<sub>3</sub>-rich UT/LS air masses. For instance the levels of TAM and CO during the event were moderately correlated with a least squares regression slope of  $0.0058 \pm 0.0021 \text{ ng m}^{-3} \text{ ppbv}^{-1}$  ( $r^2 = 0.61$ ,  $p < 0.05$ ). The TAM/CO slope is in agreement with values characteristic of Asian urban/industrial emissions. Trajectories (not shown) originated mostly from the Asian urban/industrial outflow region (Section 3.5.2) and suggested that mixing with UT/LS air masses likely occurred over the western Pacific.

In general, mixed ALRT + UT/LS high ozone events had characteristics that were intermediate between ALRT and UT/LS events (Table S1, Fig. 4). For instance, event-mean CO levels tended to be within the central 20% of the corresponding monthly distributions, while TAM levels tended to be moderately enhanced. By comparison, CO and TAM were typically enhanced with O<sub>3</sub> throughout ALRT events. Relationships between the levels of O<sub>3</sub> and CO measured during the mixed ALRT + UT/LS events ranged from very weakly anti-correlated to weakly correlated (Table S1). Our analysis is unable to precisely quantify the relative contributions of ALRT and UT/LS air masses to the O<sub>3</sub> enhancements measured during the mixed events; this would require a sophisticated simulation experiment with well defined O<sub>3</sub> source regions. The associated chemistries are particularly complex due to enhanced secondary photochemistry (e.g., Esler et al., 2001).

#### 4. Summary

From 2004–2009 a total of 25 days at Mt. Bachelor had MDA-8 O<sub>3</sub> > 70.0 ppbv. All of the high-ozone events occurred between early March and late September, corresponded with relatively dry air masses bearing WV values characteristic of the regional FT, and exhibited O<sub>3</sub>/WV anti-correlations. Furthermore, air mass backward trajectories suggested varying degrees of trans-Pacific transport in the FT. These features are consistent with minimal influence from the North American BL. Our analysis identified transport of O<sub>3</sub> rich air masses having influences from the UT/LS region, ALRT and mixed ALRT + UT/LS.

Based on their lack of association with enhanced levels of other pollutants, including CO and Hg, we identified the largest fraction ( $\sim 44\%$ ,  $n = 8$ ) of high-ozone events as being influenced primarily by transport of O<sub>3</sub>-rich air masses from the UT/LS (Fig. 5). Levels of O<sub>3</sub> and CO tended to be anti-correlated during UT/LS events and air-mass backward trajectories indicated transport from the UT. For several events, the associated trajectories were consistent with relatively rapid subsidence on final approach to MBO. The UT/LS events represented  $\sim 52\%$  ( $t = 85$ ) of the total classifiable high-

ozone event hours, which was slightly greater than their corresponding number fraction owing to the relatively long duration of the events (average of 11 h with O<sub>3</sub> > 70.0 ppbv). The 26 March 2009 UT/LS event was one of the longest in duration (16 h) and had the highest 8-hr average O<sub>3</sub> mixing ratio ( $108 \pm 9$  ppbv,  $1\sigma$ ) of all the recorded high-ozone events.

The ALRT events were characterized by mean levels of CO and TAM that were both enhanced in comparison to their corresponding monthly distributions. The levels of O<sub>3</sub> and CO tended to be correlated and the associated air mass backward trajectories were consistent with an influence from Asian continental outflow. The ALRT events accounted for  $\sim 22\%$  ( $n = 4$ ) of the total number of classifiable high-ozone events, but they represented only  $\sim 13\%$  ( $t = 21$ ) of the total number of classifiable event hours as these events tended to be relatively short (average of 5 h) in duration.

Several high-ozone events with chemical characteristics that were intermediate between those of the ALRT and UT/LS events were characterized as having mixed ALRT + UT/LS influences. An event observed on 7 July 2008, which had attributes consistent with trans-Pacific transport of boreal wildfire smoke and O<sub>3</sub>-rich UT air was discussed in detail. Our analysis provided evidence that the mixing of Asian urban/industrial emissions and O<sub>3</sub>-rich UT/LS air masses during trans-Pacific transport also contributed to the highest O<sub>3</sub> levels observed at MBO. The ALRT + UT/LS events accounted for  $\sim 33\%$  ( $n = 4$ ) of the total number of classifiable events and  $\sim 36\%$  ( $t = 59$ ) of the total number of classifiable event hours.

Our results are consistent with previous work demonstrating the importance of ALRT on O<sub>3</sub> in the lower FT over the U.S. west coast. They also are consistent with a significant influence from STE, particularly over the U.S. west coast, on enhanced O<sub>3</sub> in the lower FT in this region. Further work is required to quantify (1) the relative contributions of ALRT and UT/LS to O<sub>3</sub> levels observed during mixed ALRT + UT/LS high-ozone events, (2) the relationships between high-ozone events at MBO and surface-level O<sub>3</sub> enhancements at lower elevations, (3) the implications of our results for attainment of the O<sub>3</sub> air quality standard in the western U.S., especially as the standard is made more stringent, and (4) how the UT/LS and ALRT influences may be affected by rapid economic growth in Asia (Ohara et al., 2007) and climate change (c.f., Hegglin and Shepherd, 2009).

#### Acknowledgements

The authors would like to thank M. M. Wong at the University of Maryland for assistance in accessing the FIRMS MODIS data.

#### Role of the funding sources

This work was funded by the U.S. National Science Foundation and by the Electric Power Research Institute (EPRI). These sponsors had no role in the study design; in the collection, analysis and interpretation of data; in the writing of the report; and in the decision to submit the paper for publication.

#### Appendix. Supplementary data

Supplementary data associated with this article can be found in the online version, at doi:10.1016/j.atmosenv.2011.06.056.

#### References

- Adhikary, B., Carmichael, G.R., Kulkarni, S., Wei, C., Tang, Y., D'Allura, A., Mena-Carrasco, M., Streets, D.G., Zhang, Q., Pierce, R.B., Al-Saadi, J.A., Emmons, L.K., Pfister, G.G., Avery, M.A., Barrick, J.D., Blake, D.R., Brune, W.H., Cohen, R.C.,

- Dibb, J.E., Fried, A., Heikes, B.G., Huey, L.G., O'Sullivan, D.W., Sachse, G.W., Shetter, R.E., Singh, H.B., Campos, T.L., Cantrell, C.A., Flocke, F.M., Dunlea, E.J., Jimenez, J.L., Weinheimer, A.J., Crouse, J.D., Wennberg, P.O., Schauer, J.J., Stone, E.A., Jaffe, D.A., Reidmiller, D.R., 2010. A regional scale modeling analysis of aerosol and trace gas distributions over the eastern Pacific during the INTEX-B field campaign. *Atmospheric Chemistry and Physics* 10, 2091–2115. <http://www.atmos-chem-phys.net/10/2091/2010/>.
- Bertschi, I.T., Jaffe, D.A., Jaeglé, L., Price, H.U., Dennison, J.B., 2004. PHOBEA/ITCT 2002 airborne observations of transpacific transport of ozone, CO, volatile organic compounds, and aerosols to the northeast Pacific: impacts of Asian anthropogenic and Siberian boreal fire emissions. *Journal of Geophysical Research* 109 (D23S12). doi:10.1029/2003JD004328.
- Bertschi, I.T., Jaffe, D.A., 2005. Long-range transport of ozone, carbon monoxide, and aerosols to the NE Pacific troposphere during the summer of 2003: observations of smoke plumes from Asian boreal fires. *Journal of Geophysical Research* 110 (D05303). doi:10.1029/2004JD005135.
- Bey, I., Jacob, D.J., Logan, J.A., Yantosca, R.M., 2001. Asian chemical outflow to the Pacific in spring: origins, pathways, and budgets. *Journal of Geophysical Research* 106 (D19), 23,097–23,113.
- Bolton, D., 1980. The computation of equivalent potential temperature. *Monthly Weather Review* 108, 1046–1053.
- Brioude, J., Cooper, O.R., Trainer, M., Ryerson, T.B., Holloway, J.S., Baynard, T., Peischl, J., Warneke, C., Neuman, J.A., De Gouw, J., Stohl, A., Eckhardt, S., Frost, G.J., McKeen, S.A., Hsie, E.Y., Fehsenfeld, F.C., Nédélec, P., 2007. Mixing between a stratospheric intrusion and a biomass burning plume. *Atmospheric Chemistry and Physics* 7, 4229–4235. [www.atmos-chem-phys.net/7/4229/2007/](http://www.atmos-chem-phys.net/7/4229/2007/).
- Brown-Steiner, B., Hess, P.G. Asian influence on surface ozone in the United States: a comparison of regional chemistry, seasonality, and transport mechanisms. *Journal of Geophysical Research*, submitted for publication.
- Cooper, O.R., Forster, C., Parrish, D., Trainer, M., Dunlea, E., Ryerson, T., Hübler, G., Fehsenfeld, F., Nicks, D., Holloway, J., de Gouw, J., Warneke, C., Roberts, J.M., Flocke, F., Moody, J., 2004a. A case study of transpacific warm conveyor belt transport: influence of merging airstreams on trace gas import to North America. *Journal of Geophysical Research* 19 (D23S08). doi:10.1029/2003JD003624.
- Cooper, O., Forster, C., Parrish, D., Dunlea, E., Hübler, G., Fehsenfeld, F., Holloway, J., Oltmans, S., Johnson, B., Wimmers, A., Horowitz, L., 2004b. On the life cycle of a stratospheric intrusion and its dispersion into polluted warm conveyor belts. *Journal of Geophysical Research* 109 (D23S09). doi:10.1029/2003JD004006.
- Cooper, O.R., Parrish, D.D., Stohl, A., Trainer, M., Nédélec, P., Thouret, V., Cammas, J.P., Oltmans, S.J., Johnson, B.J., Tarasick, D., Leblanc, T., McDermid, I.S., Jaffe, D., Gao, R., Stith, J., Ryerson, T., Aikin, K., Campos, T., Weinheimer, A., Avery, A., 2010. Increasing springtime ozone mixing ratios in the free troposphere over western North America. *Nature* 463, 344–348. doi:10.1038/nature08708.
- Davies, D.K., Ilavajhala, S., Wong, M.M., Justice, C.O., 2009. Fire information for resource management system: archiving and distributing MODIS active fire data. *IEEE Transactions on Geoscience and Remote Sensing* 41 (1), 72–79.
- de Gouw, J.A., Cooper, O.R., Warneke, C., Hudson, P.K., Fehsenfeld, F.C., Holloway, J.S., Hübler, G., Nicks Jr., D.K., Nowak, J.B., Parrish, D.D., Ryerson, T.B., Atlas, E.L., Donnelly, S.G., Schauffler, S.M., Stroud, V., Johnson, K., Carmichael, G.R., Streets, D.G., 2004. Chemical composition of air masses transported from Asia to the U.S. West Coast during ITCT 2K2: fossil fuel combustion versus biomass-burning signatures. *Journal of Geophysical Research* 109 (D23S20). doi:10.1029/2003JD004202.
- Draxler, R.R., Hess, G.D., 1998. An overview of the HYSPLIT\_4 modeling system for trajectories, dispersion and deposition. *Australian Meteorological Magazine* 47, 295–308.
- Draxler, R.R., Rolph, G.D., 2011. HYSPLIT (Hybrid Single-Particle Lagrangian Integrated Trajectory) Model, access via NOAA ARL READY Website. NOAA Air Resources Laboratory, Silver Spring, MD. <http://ready.arl.noaa.gov/HYSPLIT.php>.
- Duncan, B.N., Martin, R.V., Staudt, A.C., Yevich, R., Logan, J.A., 2003. Interannual and seasonal variability of biomass burning emissions constrained by satellite observations. *Journal of Geophysical Research* 108 (D2), 4100. doi:10.1029/2002JD002378.
- Environmental Protection Agency (EPA), 2010. National Ambient Air Quality Standards for Ozone. Federal Register 75(11), Washington, DC.
- Esler, J.G., Tan, D.G.H., Haynes, P.H., Evans, M.J., Law, K.S., Plantevin, P.H., Pyle, J.A., 2001. Stratosphere-troposphere exchange: chemical sensitivity to mixing. *Journal of Geophysical Research* 106 (D5), 4717–4731.
- Finley, B.D., Swartzendruber, P.C., Jaffe, D.A., 2009. Particulate mercury emissions in regional wildfire plumes observed at the Mount Bachelor Observatory. *Atmospheric Environment* 43, 6074–6083.
- Fiore, A.M., Jacob, D.J., Bey, I., Yantosca, R.M., Field, B.D., Fusco, A.C., Wilkinson, J.G., 2002. Background ozone over the United States in summer: Origin, trend, and contribution to pollution episodes. *Journal of Geophysical Research* 107 (D15), 4257. doi:10.1029/2001JD000982.
- Fischer, E.V., Jaffe, D.A., Reidmiller, D.R., Jaeglé, L., 2010a. Meteorological controls on observed peroxyacetyl nitrate at Mount Bachelor during the spring of 2008. *Journal of Geophysical Research* 115 (D03302). doi:10.1029/2009JD012776.
- Fischer, E.V., Jaffe, D.A., Marley, N.A., Gaffney, J.S., Marchany-Rivera, A., 2010b. Optical properties of aged Asian aerosols observed over the U.S. Pacific Northwest. *Journal of Geophysical Research* 115 (D20209). doi:10.1029/2010JD013943.
- Friedli, H.R., Radke, L.F., Prescott, R., Li, P., Woo, J.H., Carmichael, G.R., 2004. Mercury in the atmosphere around Japan, Korea, and China as observed during the 2001 ACE-Asia field campaign: measurements, distributions, sources, and implications. *Journal of Geophysical Research* 109 (D19S25). doi:10.1029/2003JD004244.
- Gustin, M., Jaffe, D., 2010. Reducing the uncertainty in measurement and understanding of mercury in the atmosphere. *Environmental Science and Technology* 44, 2222–2227.
- Hegglin, M.I., Shepherd, T.G., 2009. Large climate-induced changes in ultraviolet index and stratosphere-to-troposphere ozone flux. *Nature* 2, 687–691. doi:10.1038/NGEO0604.
- Hoor, P., Fischer, H., Lange, L., Lelieveld, J., 2002. Seasonal variations of a mixing layer in the lowermost stratosphere as identified by the CO–O<sub>3</sub> correlation from in situ measurements. *Journal of Geophysical Research* 197 (D4), 4044. doi:10.1029/2000JD000289.
- Huang, M., Carmichael, G.R., Kulkarni, S., Spak, S.N., Chai, T., Oltmans, S.J., Jaffe, D.A., Streets, D.G., Kaduwela, A., Weinheimer, A.J., Huey, G.L. Source attribution at western U.S. receptors and the impacts of transported background pollutants and local fires on surface air quality. *Journal of Geophysical Research*, submitted for publication.
- Hudman, R.C., Jacob, D.J., Cooper, O.R., Evans, M.J., Heald, C.L., Park, R.J., Fehsenfeld, F., Flocke, F., Holloway, J., Hübler, G., Kita, K., Koike, M., Kondo, Y., Neuman, A., Nowak, J., Oltmans, S., Parrish, D., Roberts, J.M., Ryerson, T., 2004. Ozone production in transpacific Asian pollution plumes and implications for ozone air quality in California. *Journal of Geophysical Research* 109 (D23S10). doi:10.1029/2004JD004974.
- Jacob, D.J., Logan, J.A., Murti, P.P., 1999. Effect of rising Asian emissions on surface ozone in the United States. *Geophysical Research Letters* 26, 2175–2178.
- Jaeglé, L., Jaffe, D.A., Price, H.U., Weiss-Penzias, P., Palmer, P.L., Evans, M.J., Jacob, D.J., Bey, I., 2003. Sources and budgets for CO and O<sub>3</sub> in the northeastern Pacific during the spring of 2001: results from the PHOBEA-II Experiment. *Journal of Geophysical Research* 108 (D20), 8802. doi:10.1029/2002JD003121.
- Jaffe, D., Anderson, T., Covert, D., Kotchenruther, B., Bernsten, T., Danielson, J., Simpson, W., Bernsten, T., Karlsdottir, S., Blake, D., Harris, J., Carmichael, G., Uno, I., 1999. Transport of Asian air pollution to North America. *Geophysical Research Letters* 26 (6), 711–714.
- Jaffe, D.J., Bertschi, I., Jaeglé, L., Novelli, P., Reid, J.S., Tanimoto, H., Vingarzan, R., Westphal, D.L., 2004. Long-range transport of Siberian biomass burning emissions and impact on surface ozone in western North America. *Geophysical Research Letters* 32 (L16106). doi:10.1029/2004GL020093.
- Jaffe, D.A., Prestbo, E., Swartzendruber, P., Weiss-Penzias, P., Kato, S., Takami, A., Hatakeyama, W., Kajii, Y., 2005. Export of atmospheric mercury from Asia. *Atmospheric Environment* 39, 3029–3038.
- Jaffe, D., Ray, J., 2007. Increase in surface ozone at rural sites in the western US. *Atmospheric Environment* 41, 5452–5463.
- Justice, C.O., Giglio, L., Korontzi, S., Owens, J., Morisette, J.T., Roy, D., Desloires, J., Alleaume, S., Petitcolin, F., Kaufman, Y., 2002. The MODIS fire products. *Remote Sensing of Environment* 83, 244–262.
- Kentarchos, A.S., Roelofs, G.J., 2003. A model study of stratospheric ozone in the troposphere and its contribution to tropospheric OH formation. *Journal of Geophysical Research* 108 (D12), 8517. doi:10.1029/2002JD002598.
- Kim, C.S., Alexis, N.E., Rappold, A.G., Kehrl, H., Hazucha, M.J., Lay, J.C., Schmitt, M.T., Case, M., Devlin, R.B., Peden, D.B., Diaz-Sanchez, D., 2011. Lung function and inflammatory responses in healthy young adults exposed to 0.06 ppm ozone for 6.6 hours. *American Journal of Respiratory and Critical Care Medicine* 183, 1215–1221. doi:10.1164/rccm.201011-1813OC.
- Kotchenruther, R.A., Jaffe, D.A., Jaeglé, L., 2001. Ozone photochemistry and the role of peroxyacetyl nitrate in the springtime northeastern Pacific troposphere: results from the Photochemical Ozone Budget of the Eastern North Pacific Atmosphere (PHOBEA) campaign. *Journal of Geophysical Research* 106 (D22), 28,731–28,742.
- Landis, M.S., Stevens, R.K., Schaedlich, F., Prestbo, E.M., 2002. Development and characterization of an annular denuder methodology for the measurement of divalent inorganic reactive gaseous mercury in ambient air. *Environmental Science and Technology* 36, 3000–3009.
- Langford, A.O., Senff, C.J., Alvarez II, R.J., Banta, R.M., Brewer, A., Hardesty, R., Brioude, J., Cooper, O.R., 2010. Elevated ozone layers in the lower free troposphere during CalNex. Abstract A23D-02 presented at 2010 Fall Meeting, AGU, San Francisco, Calif., 13–17 Dec.
- Liang, Q., Jaeglé, L., Wallace, J.M., 2005. Meteorological indices for Asian outflow and transpacific transport on daily to interannual timescales. *Journal of Geophysical Research* 110 (D18308). doi:10.1029/2005JD005788.
- Lin, M., Holloway, T., Carmichael, G.R., Fiore, A.M., 2010. Quantifying pollution inflow and outflow over East Asia in spring with regional and global models. *Atmospheric Chemistry and Physics* 10, 4221–4239. doi:10.1029/2002JD003102.
- Liu, H., Jacob, D.J., Bey, I., Yantosca, R.M., Duncan, B.N., Sachse, G.W., 2003. Transport pathways for Asian pollution outflow over the Pacific: interannual and seasonal variations. *Journal of Geophysical Research* 108 (D20), 8786. doi:10.1029/2002JD003102.
- Lyman, S.N., Gustin, M.S., 2008. Speciation of atmospheric mercury at two sites in northern Nevada, USA. *Atmospheric Environment* 42, 927–939.
- Lyman, S.N., Gustin, M.S., 2009. Determinants of atmospheric mercury concentrations in Reno, Nevada, U.S.A. *Science of the Total Environment* 408, 431–438.
- McDonald-Buller, E.C., Allen, D.T., Brown, N., Jacob, D., Jaffe, D., Kolb, C., Lefohn, A., Oltmans, S., Parrish, D., Yarwood, G. Establishing Policy Relevant Background (PRB) ozone concentrations in the United States. *Atmospheric Environment*, submitted for publication.

- Newchurch, M.J., Ayoub, M.A., Oltmans, S., Johnson, B., Schmidlin, F.J., 2003. Vertical distribution of ozone at four sites in the United States. *Journal of Geophysical Research* 108 (D1), 4031. doi:10.1029/2002JD002059.
- Novelli, P.C., Steele, L., PaulTans, P.P., 1992. Mixing ratios of carbon monoxide in the troposphere. *Journal of Geophysical Research* 97 (D18), 20,731–20,750.
- NRC, 2010. *Global Sources of Local Pollution: An Assessment of Long-Range Transport of Key Air Pollutants to and from the United States*. The National Academies Press, Washington, DC, USA.
- Ohara, T., Akimoto, H., Kurokawa, J., Horii, N., Yamaji, K., Yan, X., Hayasaka, T., 2007. An Asian emission inventory of anthropogenic emission sources for the period 1980–2020. *Atmospheric Chemistry Physics* 7, 4419–4444. [www.atmos-chem-phys.net/7/4419/2007/](http://www.atmos-chem-phys.net/7/4419/2007/).
- Peterson, C., Gustin, M., 2008. Mercury in the air, water and biota at the Great Salt Lake (Utah, USA). *Science of the Total Environment* 405, 255–268.
- Price, H.U., Jaffe, D.A., Cooper, O.R., Doskey, P.V., 2004. Photochemistry, ozone production, and dilution during long-range transport episodes from Eurasia to the northwest United States. *Journal of Geophysical Research* 109 (D23S13). doi:10.1029/2003JD004400.
- Reidmiller, D.R., Jaffe, D.A., Chand, D., Strode, S., Swartzendruber, P., Wolfe, G.M., Thornton, J.A., 2009. Interannual variability of long-range transport as seen at the Mt. Bachelor observatory. *Atmospheric Chemistry and Physics* 9, 55–572. <http://www.atmos-chem-phys.net/9/557/2009/>.
- Reidmiller, D.R., Jaffe, D.A., Fischer, E.V., Finley, B., 2010. Nitrogen oxides in the boundary layer and free troposphere at the Mt. Bachelor Observatory. *Atmospheric Chemistry and Physics* 10, 6043–6062. <http://www.atmos-chem-phys.net/10/6043/2010/>.
- Sheu, G.R., Lin, N.H., Wang, J.L., Lee, C.T., Yang, C.F.O., Wang, S.H., 2010. Temporal distribution and potential sources of atmospheric mercury measured at a high-elevation background station in Taiwan. *Atmospheric Environment* 44, 2393–2400.
- Sprenger, M., Wernli, H., 2003. A northern hemispheric climatology of cross-tropopause exchange for the ERA15 time period (1979–1993). *Journal of Geophysical Research* 108 (D12), 8521. doi:10.1029/2002JD002636.
- Stohl, A., Spichtinger-Rakowsky, N., Bonasoni, P., Feldmann, H., Memmesheimer, M., Scheel, H.E., Trickl, T., Hübener, S., Ringer, W., Mandl, M., 2000. The influence of stratospheric intrusions on alpine ozone concentrations. *Atmospheric Environment* 34, 1323–1354.
- Stohl, A., Eckhardt, S., Forster, C., James, P., Spichtinger, N., 2002. On the pathways and timescales of intercontinental air pollution transport. *Journal of Geophysical Research* 107 (D23), 4684. doi:10.1029/2001JD001396.
- Swartzendruber, P.C., Jaffe, D.A., Prestbo, E.M., Weiss-Penzias, P., Selin, N.E., Park, R., Jacob, D.J., Strode, S., Jaeglé, L., 2006. Observations of reactive gaseous mercury in the free troposphere at the Mount Bachelor Observatory. *Journal of Geophysical Research* 111 (D24301). doi:10.1029/2006JD007415.
- Tang, Q., Prather, M.J., 2010. Correlating tropospheric column ozone with tropopause folds: the Aura-OMI satellite data. *Atmospheric Chemistry and Physics* 10, 9681–9688. <http://www.atmos-chem-phys.net/10/9681/2010/>.
- Tanimoto, H., 2009. Increase in springtime tropospheric ozone at a mountainous site in Japan for the period 1998–2006. *Atmospheric Environment* 43, 1258–1363.
- Tanimoto, H., Matsumoto, K., Uematsu, M., 2008. Ozone-CO correlations in Siberian wildfire plumes observed at Rishiri Island. *Scientific Online Letters on the Atmosphere* 4, 65–68. doi:10.2151/sola/2008-017.
- Tanimoto, H., Ohara, T., Uno, I., 2009. Asian anthropogenic emissions and decadal trends in springtime tropospheric ozone over Japan: 1998–2007. *Geophysical Research Letters* 36 (L23802). doi:10.1029/2009GL041382.
- Tilmes, S., Pan, L.L., Hoor, P., Atlas, E., Avery, M.A., Campos, T., Christensen, L.E., Diskin, G.S., Gao, R.S., Herman, R.L., Hints, E.J., Loewenstein, M., Lopez, J., Paige, M.E., Pittman, J.V., Podolske, J.R., Proffitt, M.R., Sachse, G.W., Schiller, C., Schlager, H., Smith, J., Spelten, N., Webster, C., Weinheimer, A., Zondlo, M.A., 2010. An aircraft-based upper troposphere lower stratosphere O<sub>3</sub>, CO, and H<sub>2</sub>O climatology for the Northern Hemisphere. *Journal of Geophysical Research* 115 (D14303). doi:10.1029/2009JD012731.
- Val Martín, M., Honrath, R.E., Owen, R.C., Pfister, G., Fialho, P., Barata, F., 2006. Significant enhancements of nitrogen oxides, black carbon, and ozone in the North Atlantic lower free troposphere resulting from North American boreal wildfires. *Journal of Geophysical Research* 111 (D23S60). doi:10.1029/2006JD007530.
- Weiss-Penzias, P., Jaffe, D.A., Swartzendruber, P., Dennison, J.B., Chand, D., Hafner, W., Prestbo, E., 2006. Observations of Asian air pollution in the free troposphere at Mount Bachelor Observatory during the spring of 2004. *Journal of Geophysical Research* 111 (D10304). doi:10.1029/2005JD006522.
- Weiss-Penzias, P., Jaffe, D., Swartzendruber, P., Hafner, W., Chand, D., Prestbo, E., 2007. Quantifying Asian and biomass burning sources of mercury using the Hg/CO ratio in pollution plumes observed at the Mount Bachelor observatory. *Atmospheric Environment* 41, 4366–4379.
- Whittlestone, S., Zahorowski, W., 1998. Baseline radon detectors for shipboard use: Development and deployment in the First Aerosol Characterization Experiment (ACE 1). *Journal of Geophysical Research* 103 (D13), 16,743–16,751.
- Wolfe, G.M., Thornton, J.A., McNeill, V.F., Jaffe, D.A., Reidmiller, D., Chand, D., Smith, J., Swartzendruber, P., Flocke, F., Zheng, W., 2007. Influence of trans-Pacific pollution transport on acyl peroxy nitrate abundances and speciation at Mount Bachelor Observatory during INTEX-B. *Atmospheric Chemistry and Physics* 7, 5309–5325. <http://www.atmos-chem-phys.net/7/5309/2007/>.
- Yienger, J.J., Galanter, M., Holloway, T.A., Phadnis, M.J., Guttikunda, S.K., Carmichael, G.R., Moxim, W.J., Levy II, H., 2000. The episodic nature of air pollution transport from Asia to North America. *Journal of Geophysical Research* 105 (D22), 26,931–26,945.
- Zhang, L., Jacob, D.J., Boersma, K.F., Jaffe, D.A., Olson, J.R., Bowman, K.W., Worden, J.R., Thompson, A.M., Avery, M.A., Cohen, R.C., Dibb, J.E., Flock, F.M., Fuelberg, H.E., Huey, L.G., McMillan, W.W., Singh, H.B., Weinheimer, A.J., 2008. Transpacific transport of ozone pollution and the effect of recent Asian emission increases on air quality in North America: an integrated analysis using satellite, aircraft, ozonesonde, and surface observations. *Atmospheric Chemistry and Physics* 8, 6117–6136. <http://www.atmos-chem-phys.net/8/6117/2008/>.
- Zhang, L., Jacob, D.J., Kopacz, M., Henze, D.K., Singh, K., Jaffe, D.A., 2009. Intercontinental source attribution of ozone pollution at western U.S. sites using an adjoint method. *Geophysical Research Letters* 36 (L11810). doi:10.1029/2009GL037950.